


UTILIZATION OF PALM OIL FUEL ASH AS SILICA SOURCE OF NI/SBA-15 FOR CARBON DIOXIDE REFORMING OF METHANE

(PENGUNAAN ABU BAHAN API KELAPA SAWIT SEBAGAI SUMBER SILIKA BAGI NI/SBA-15 UNTUK KARBON DIOKSIDA PEMBAHARUAN METANA)



**HERMA DINA SETIABUDI
AISHAH ABDUL JALIL
CHIN SIM YEE
NURUL AINI MOHAMED RAZALI**

**RESEARCH VOTE NOM:
RDU151414**

UMP

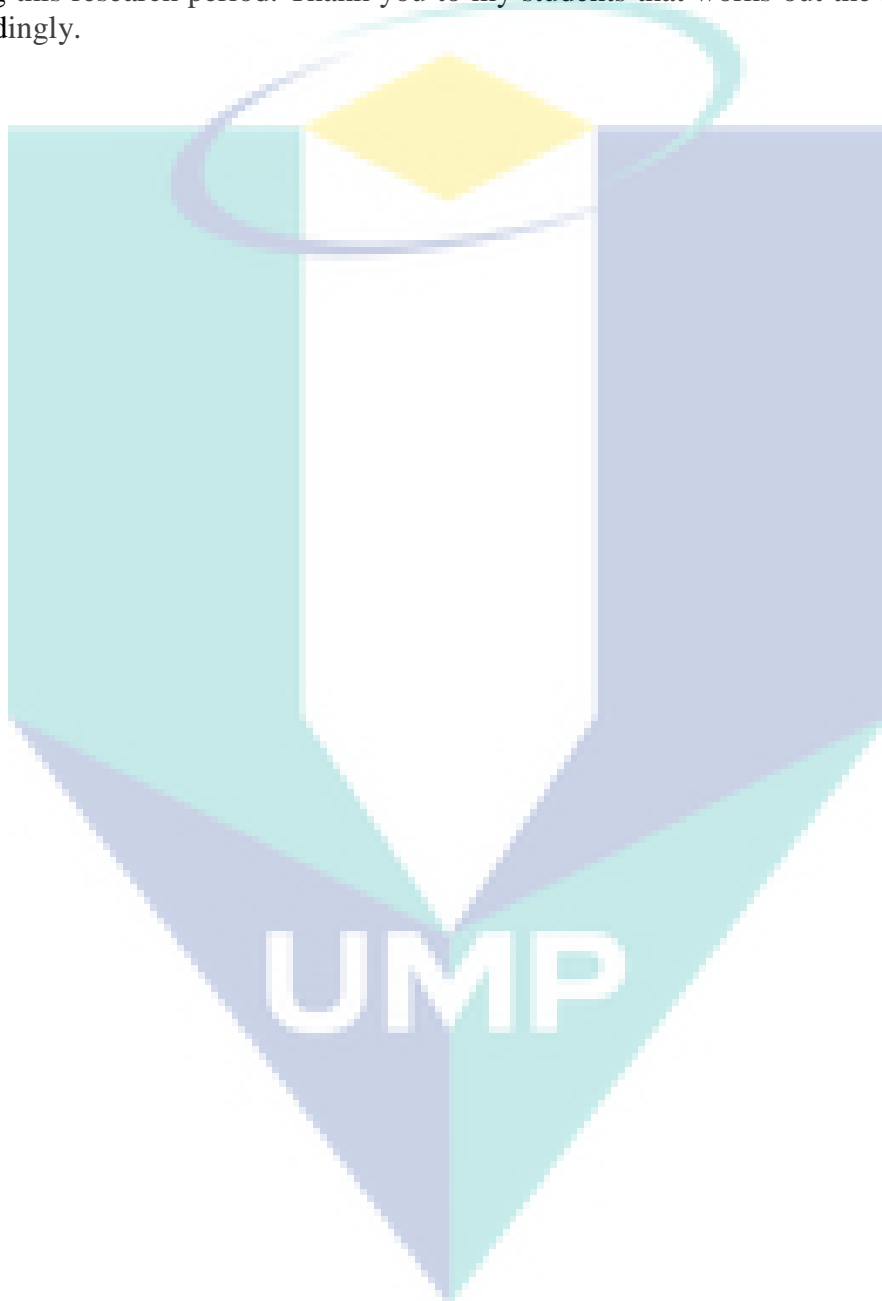
Faculty of Chemical & Natural Resources Engineering

Universiti Malaysia Pahang

2018

ACKNOWLEDGEMENTS

I would like to acknowledge Ministry of Education Malaysia for funding this research activity through Research Acculturation Grant Scheme RDU151414 and Chemical Engineering Laboratory, FKKSA, UMP for equipment and facilities available. I also would like to extend my gratitude to team members who always help and gave advice during this research period. Thank you to my students that works out the research plan accordingly.



ABSTRACT

UTILIZATION OF PALM OIL FUEL ASH AS SILICA SOURCE OF Ni/SBA-15 FOR CARBON DIOXIDE REFORMING OF METHANE

(Keywords: Ni/SBA-15, CO₂ dry reforming; POFA)

Climate change has become one of the main concerns of humanity in recent century. As carbon dioxide (CO₂) and methane (CH₄) are considered as the main contributor to greenhouse gases (GHGs), the transformation of these two gases into more valuable products (syngas) by CO₂ reforming of CH₄ (CRM) has been attracted extensive attention. CRM has been studied extensively using variety of supported metal catalysts including Ni/SBA-15. However, the cost for the large-scale manufacture of SBA-15 is high, owing to the cost of both templates and silica sources. Therefore, the objective is to synthesis the Ni/SBA-15 using palm oil fuel ash (POFA) as a silica source for CRM. The preparation of POFA sodium silicate (POFA-Na₂SiO₃) was done using sodium hydroxide (NaOH) fusion method under several parameters including NaOH/POFA mass ratio, fusion temperature and H₂O/NaOH-fused POFA mass ratio. The optimum condition was achieved at NaOH/POFA mass ratio of 2:1, fusion temperature of 550°C and H₂O/NaOH-fused POFA mass ratio of 4:1, with maximum silica content of 40570 ppm. The obtained POFA-Na₂SiO₃ was used as the silica source for the synthesis of Ni/SBA-15(POFA) by studying the effect of Na₂SiO₃-POFA/P123 mass ratios (2.0, 2.9 and 4.0) and Ni loadings (1-5 wt%). The effect of Na₂SiO₃-POFA/P123 ratios revealed that the optimal synthesis ratio was at 2.9, which produces a well-defined hexagonal framework, smaller NiO particles, stronger Ni-support interaction, homogeneous metal distribution and higher amount of basic sites. The effect of Ni loadings revealed that the highest catalytic performance and stability was marked by 3wt% owing to the well dispersion Ni particles on the SBA-15 surfaces that creates a good metal-support interaction (Ni-O-Si) and considerable amount of basic sites, which then enhances its catalytic performance. This study affirmed that POFA can be served as silica substitution of Ni/SBA-15. Optimal Ni/SBA-15 was found at Na₂SiO₃-POFA/P123 ratio of 2.9 and Ni loading of 3wt%, with CH₄ conversion = 87.11%, CO₂ conversion = 76.51%, H₂/CO = 0.84.

Key researchers: Herma Dina Setiabudi, Aishah Abdul Jalil, Chin Sim Yee, Nurul Aini Mohamed Razali

E-mail : herma@ump.edu.my; Tel. No.: 09-5492836; Vote No.: RDU151414

ABSTRAK

PENGGUNAAN ABU BAHAN API KELAPA SAWIT SEBAGAI SUMBER SILIKA BAGI Ni/SBA-15 UNTUK KARBON DIOKSIDA PEMBAHARUAN METANA

(Kata Kunci: Ni/SBA-15, pembaharuan kering CO₂; POFA)

Perubahan iklim telah menjadi salah satu **keimbangan** yang utama dalam abad kebelakangan ini. Oleh kerana karbon dioksida (CO₂) dan metana (CH₄) adalah penyumbang utama kepada gas rumah hijau (GHG), transformasi kedua-dua gas ke kepada produk yang lebih berharga (syngas) oleh CO₂ pembaharuan CH₄ (CRM). CRM telah dikaji secara meluas menggunakan pelbagai pemangkin logam yang disokong termasuk Ni/SBA-15. Walau bagaimanapun, kos untuk pengeluaran SBA-15 secara besar-besaran adalah tinggi, disebabkan oleh kos kedua-dua templat dan sumber silika. Oleh itu, matlamat kajian ini adalah untuk sintesis Ni/SBA-15 menggunakan abu bahan api kelapa sawit (POFA) sebagai sumber silika untuk CRM. Penyediaan POFA natrium silikat (POFA-Na₂SiO₃) dilakukan menggunakan kaedah gabungan natrium hidroksida (NaOH) di bawah beberapa parameter termasuk nisbah jisim NaOH/POFA, suhu gabungan dan nisbah jisim POFA bersalut H₂O/NaOH. Keadaan optima dicapai pada nisbah jisim NaOH/POFA 2:1, suhu gabungan 550°C dan nisbah jisim POFA bersalut H₂O/NaOH 4:1, dengan kandungan silika maksimum 40570 ppm. POFA-Na₂SiO₃ yang diperolehi digunakan sebagai sumber silika untuk sintesis Ni/SBA-15(POFA) dengan mengkaji kesan nisbah jisim Na₂SiO₃-POFA/P123 (2.0, 2.9 dan 4.0) dan beban Ni (1-5 wt %). Kesan nisbah Na₂SiO₃-POFA/P123 mendedahkan bahawa nisbah sintesis optima berada pada 2.9, yang menghasilkan rangka kerja heksagon yang jelas, zarah NiO yang lebih kecil, interaksi Ni-sokongan yang lebih kuat, pengedaran logam homogen dan jumlah tapak asas yang lebih tinggi. Kesan beban Ni mendedahkan bahawa prestasi dan kestabilan katalitik tertinggi ditandakan dengan 3wt% disebabkan oleh zarah Ni penyebaran baik pada permukaan SBA-15 yang menghasilkan interaksi sokongan logam yang baik (Ni-O-Si) dan jumlah yang besar tapak asas, yang kemudiannya meningkatkan prestasi pemangkinnya. Kajian ini menegaskan bahawa POFA boleh digunakan sebagai pengganti silika Ni/SBA-15. Optimal Ni/SBA-15 didapati pada nisbah Na₂SiO₃-POFA/P123=2.9 dan beban Ni = 3wt%, dengan penukaran CH₄ = 87.11%, penukaran CO₂ = 76.51%, H₂/CO = 0.84.

Penyelidik utama: Herma Dina Setiabudi, Aishah Abdul Jalil, Chin Sim Yee, Nurul Aini
Mohamed Razali

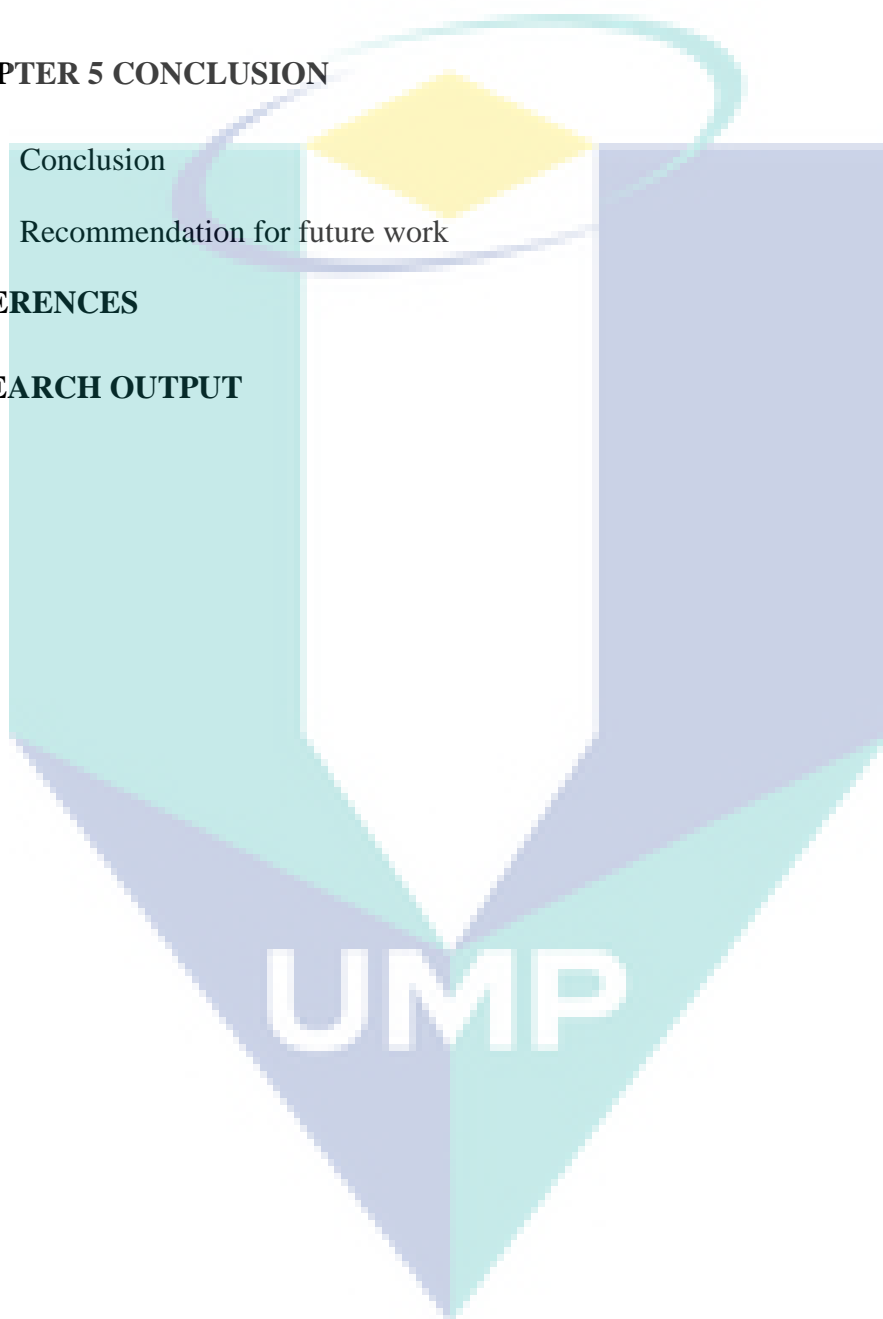
E-mail : herma@ump.edu.my; Tel. No.: 09-5492836; Vote No.: RDU151414

TABLE OF CONTENT

TITLE PAGE	i
ACKNOWLEDGEMENTS	ii
ABSTRACT	iii
ABSTRAK	iv
TABLE OF CONTENT	v
LIST OF TABLES	viii
LIST OF FIGURES	ix
LIST OF SYMBOLS	xi
LIST OF ABBREVIATIONS	xii
CHAPTER 1 INTRODUCTION	1
1.1 Background of the study	1
1.2 Objectives	3
1.3 Scopes of the study	3
CHAPTER 2 LITERATURE REVIEW	5
2.1 Introduction	5
2.2 Carbon cycle	7
2.2.1 Carbon cycle, Global Warming, and Greenhouse Gases	7
2.2.2 Previous effort options to decrease CO ₂ emission	8
2.2.3 Catalytic reforming of methane with CO ₂	10
2.3 Syngas	12
2.4 Waste materials as silica source	14

2.5	Previous studies on CO ₂ reforming catalysts	19
2.6	Mesoporous materials as catalytic support	21
CHAPTER 3 METHODOLOGY		25
3.1	Chemicals	25
3.2	Preparation of POFA sodium silica solution	25
3.3	Synthesis of SBA-15 support	26
3.4	Preparation of Ni/SBA-15	27
3.5	Catalyst characterization	27
3.6	CO ₂ reforming of CH ₄	28
CHAPTER 4 RESULTS AND DISCUSSION		30
4.1	Effect of extraction parameter on concentration of extracted silica	30
4.1.1	Effect of mass ratio of NaOH/POFA	30
4.1.2	Effect of fusion temperature	31
4.1.3	Effect of mass ratio of H ₂ O/NaOH-fused POFA	32
4.1.4	Outcomes of the study	32
4.2	Effect of Na ₂ SiO ₃ -POFA/P123 mass ratios on the properties and catalytic activity of Ni/SBA-15 towards CO ₂ reforming of CH ₄	32
4.2.1	Characterization of the catalyst	33
4.2.2	Catalytic performance of the catalyst toward CO ₂ reforming of CH ₄	41
4.2.3	Outcomes of the study	44
4.3	Effect of Ni-Loading on the properties and catalytic activity of Ni/SBA-15 towards CO ₂ reforming of CH ₄	45
4.3.1	Characterization of the catalyst	45

4.3.2	Catalytic performance of the catalyst towards CO ₂ reforming of CH ₄	52
4.3.3	Deactivation of catalyst	55
4.3.4	Outcomes of the study	57
CHAPTER 5 CONCLUSION		58
5.1	Conclusion	58
5.2	Recommendation for future work	59
REFERENCES		60
RESEARCH OUTPUT		66



LIST OF TABLES

Table 2:1	Processes Producing Syngas	13
Table 2:2	Chemical Properties of RHA after burning out	15
Table 2:3	Chemical Properties of Sugarcane Bagasse after Acid Treatment with Oxygen	15
Table 2:4	Chemical Composition of Fly Ash	16
Table 2:5	Physical Characteristics of the Raw and Processed POFA	17
Table 2:6	Chemical Composition of POFA	17
Figure 2:9	POFA dumped as waste	18
Table 2:7	Types of Waste Materials as Silica Source	18
Table 2:8	Relative activities for steam reforming of methane, $T = 550^{\circ}\text{C}$, $S/C = 4$, $P = 1$ bar	20
Table 2:9	Types of Metal Loading	20
Table 2:10	Melting Point of Metal Oxides as Catalyst Support	23
Table 2:11	Types of Catalytic Support	24
Table 3:1	List of chemicals	25
Table 4:1	Physical attributes of Ni/SBA-15(Comm.) and Ni/SBA-15 with Na_2SiO_3 -POFA/P123 mass ratios of 2.0, 2.9 and 4.0.	34
Table 4:2	Physical properties of SBA-15, 1Ni/SBA-15, 2Ni/SBA-15, 3Ni/SBA-15 and 5Ni/SBA-15.	47
Table 4:3	Amount CO_2 -TPD of SBA-15, 1Ni/SBA-15, 2Ni/SBA-15, 3Ni/SBA-15 and 5Ni/SBA-15.	51

LIST OF FIGURES

Figure 2:1	Proposed surface mechanism for CO ₂ reforming of CH ₄	6
Figure 2:2	The Carbon Cycle	8
Figure 2:3	CO ₂ recovery from flue gas for enhanced methanol production.	9
Figure 2:4	Schematic Diagram of CO ₂ reforming of Methane	12
Figure 2:5	The Chemical Energy Transmission System (CETS)	12
Figure 2:6	Main usage areas of syngas	13
Figure 2:7	Synthesis Routes of Producing Syngas	14
Figure 2:8	Incinerator producing POFA	18
Figure 2:10	Schematic diagram of SBA-15	24
Figure 3:1	Process flow diagram of the CO ₂ reforming of CH ₄ . (1) Regulator, (2) valve, (3) mass flow controller, (4) gas chamber, (5) vertical tube furnace, (6) temperature controller, (7) condenser	29
Figure 4:1	Effect of NaOH/POFA mass ratio on concentration of extracted silica	31
Figure 4:2	Effect of fusion temperature on concentration of extracted silica.	31
Figure 4:3	Effect of H ₂ O/NaOH-fused POFA mass ratio on concentration of extracted silica.	32
Figure 4:4	XRD pattern of Ni/SBA-15(Comm.) and Ni/SBA-15 with Na ₂ SiO ₃ -POFA/P123 mass ratios of 2.0, 2.9 and 4.0.	33
Figure 4:5	(A) N ₂ adsorption/desorption isotherms and (B) pore size distribution of Ni/SBA-15(Comm.) and Ni/SBA-15 with Na ₂ SiO ₃ -POFA/P123 mass ratios of 2.0, 2.9 and 4.0.	36
Figure 4:6	SEM micrographs of Ni/SBA-15 with Na ₂ SiO ₃ -POFA/P123 mass ratios of (a) 2.0, (b) 2.9 and (c) 4.0.	37
Figure 4:7	TEM micrographs of Ni/SBA-15 with Na ₂ SiO ₃ -POFA/P123 mass ratios of (a) 2.0, (b) 2.9 and (c) 4.0.	38
Figure 4:8	FTIR spectra Ni/SBA-15(Comm.) and Ni/SBA-15 with Na ₂ SiO ₃ -POFA/P123 mass ratios of 2.0, 2.9 and 4.0.	39
Figure 4:9	IR spectra of pyrrole adsorbed on activated (A) Ni/SBA-15(Comm.) and (B) Ni/SBA-15(R2.9) at (a) room temperature followed by outgassing at (b) room temperature, (c) 50°C, (d) 100°C, (e) 150°C and (f) 200°C.	40
Figure 4:10	Formation mechanism on the effect of POFA-Na ₂ SiO ₃ /P123 mass ratio over SBA-15.	41
Figure 4:11	(A) Effect of different catalysts on the CH ₄ conversion, CO ₂ conversion and H ₂ selectivity. (B) CH ₄ conversion and (C) CO ₂ conversion of Ni/SBA-15(Comm.), Ni-SBA-15(R2.0), Ni-SBA-15(R2.9) and Ni-SBA-15(R4.0) towards 24 h time-on-stream	

(TOS). Reaction conditions: GHSV = 15,000 mLg⁻¹h⁻¹, F = 50 mL/min, CH₄:CO₂=1:1, T = 800°C, P = 1 atm. 42

Figure 4:12 (A) Low and (B) Wide angle of XRD patterns of (a) SBA-15, (b) 1Ni/SBA-15, (c) 2Ni/SBA-15, (d) 3Ni/SBA-15 and (e) 5Ni/SBA-15 46

Figure 4:13 Nitrogen adsorption isotherm of (a) SBA-15, (b) 1Ni/SBA-15, (c) 2Ni/SBA-15, (d) 3Ni/SBA-15 and (e) 5Ni/SBA-15 48

Figure 4:14 FTIR spectra in the range of (A) 1400-500 cm⁻¹ and (B) 3800-3300 cm⁻¹ of (a) SBA-15, (b) 1Ni/SBA-15, (c) 2Ni/SBA-15, (d) 3Ni/SBA-15 and (e) 5Ni/SBA-15. 49

Figure 4:15 TEM images of a) SBA-15, (b) 1Ni/SBA-15, (c) 2Ni/SBA-15, (d) 3Ni/SBA-15 and (e) 5Ni/SBA-15 50

Figure 4:16 CO₂-TPD profile of a) SBA-15, (b) 1Ni/SBA-15, (c) 2Ni/SBA-15, (d) 3Ni/SBA-15 and (e) 5Ni/SBA-15. 51

Figure 4:17 (A) CH₄ conversion and (B) CO₂ conversion of Ni/SBA-15 catalysts in CO₂ reforming of CH₄. (C) Effect of different nickel loading on the CH₄ conversion, CO₂ conversion, and H₂/CO ratio. (Reaction conditions: 800°C, CH₄:CO₂:N₂=1:1:1) 55

Figure 4:18 XRD pattern of spent catalyst (a) 1Ni/SBA-15, (b) 2Ni/SBA-15, (c) 3Ni/SBA-15 and (d) 5Ni/SBA-15 56

UMP

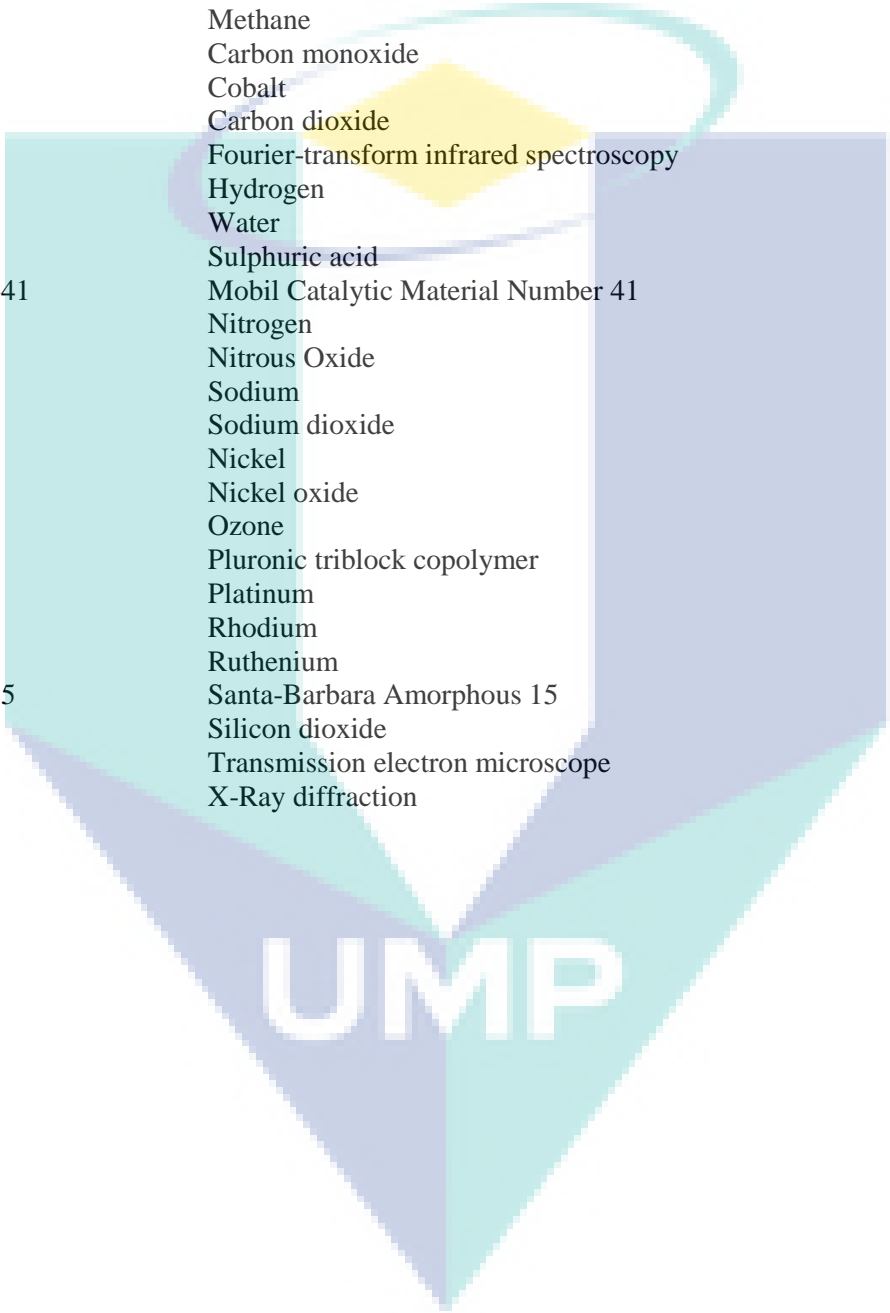
LIST OF SYMBOLS

%	Percentage
wt%	Weight percentage
ml	millilitre
θ	Angle
X_{CO_2}	Conversion of carbon dioxide
X_{CH_4}	Conversion of methane
F	Molar flow rate
P	Partial pressure
P_s	Saturated pressure
A	Area
m	Mass
λ	Wavelength of ray
$^{\circ}C$	Degrees Celsius
kg	kilogram
g	gram
h	hour
mL	milliliter
min	minute

The logo for UMPU is a large, downward-pointing arrow shape. It is composed of four triangular sections meeting at a central point. The top-left and bottom-right sections are light blue, the top-right and bottom-left sections are light purple, and the central point is white. The letters 'UMPU' are written in a bold, white, sans-serif font across the center of the arrow.

UMPU

LIST OF ABBREVIATIONS



Al ₂ O ₃	Aluminium oxide
BET	Breneuer-Emmett Teller
CH ₄	Methane
CO	Carbon monoxide
Co	Cobalt
CO ₂	Carbon dioxide
FTIR	Fourier-transform infrared spectroscopy
H ₂	Hydrogen
H ₂ O	Water
H ₂ SO ₄	Sulphuric acid
MCM-41	Mobil Catalytic Material Number 41
N ₂	Nitrogen
N ₂ O	Nitrous Oxide
Na	Sodium
Na ₂ O ₃	Sodium dioxide
Ni	Nickel
NiO	Nickel oxide
O ₃	Ozone
P123	Pluronic triblock copolymer
Pt	Platinum
Rh	Rhodium
Ru	Ruthenium
SBA-15	Santa-Barbara Amorphous 15
SiO ₂	Silicon dioxide
TEM	Transmission electron microscope
XRD	X-Ray diffraction

CHAPTER 1

INTRODUCTION

1.1 Background of the study

Global warming issue remains one of the main concerns of humanity in recent century. Greenhouse gases (GHGs) such as methane (CH₄) and carbon dioxide (CO₂) are the major contributors of global warming, researchers have proposed and investigated multitudinous solutions for the utilization of CO₂ and/or CH₄ to valuable products, such as steam reforming (Angeli et al., 2016), and CO₂ reforming of CH₄ (Bukhari et al., 2017; Setiabudi et al., 2018). Undoubtedly, the CO₂ reforming of CH₄ emerged as marvellous discovery to produce syngas (CO + H₂) from the utilization of two main greenhouse gases (CH₄ and CO₂). Excitingly, the syngas yielded from this process is a building block to synthesize the carbonyl or for Fischer-Tropsch synthesis (Setiabudi et al., 2017)

CO₂ reforming of CH₄ has been reported comprehensively by adopting a diversity of metal supported catalysts. However, Ni-supported catalysts are certified to be the most convincing candidate from an industrial prospect as they possess high catalytic performance, readily available and worthwhile (Liu et al., 2009; Pakhare et al., 2013; Sidik et al., 2016). On the other side, supports play crucial role in the catalytic performance improvement and carbon formation inhibition for CO₂ reforming of CH₄ (Usman et al., 2015). Mesoporous silica materials such as SBA-15, HMS-5, MCM-41, and FSM-16 have been in a predominant position in the past few decades with the substantial invention, development and modifications have been paid (Usman et al., 2015). Among them, mesoporous SBA-15 is preferred owing to its uniformly aligned mesopores, very high specific surface area and high thermal endurance (Abdullah et al., 2010). There are several types of silica precursors have been widely used for SBA-15 synthesis including tetraethyl orthosilicate (SiC₈H₂₀O₄, TEOS) (Fulvio et al., 2005) and sodium silicate (Na₂SiO₃) (Fulvio et al., 2005; J. Wang et al., 2013). However, these

commercial silica precursors are relatively higher in price and non-environmental friendly, thus the idea of preparing SBA-15 in a low-cost green approach has risen by employing waste material as an alternative silica precursor.

Recently, the utilization of waste material such as rice husk ash (Bhagiyalakshmi et al., 2010b, 2010a), fly ash (Gupta et al., 2017), sugarcane bagasse (Arumugam & Ponnusami, 2015) which constitute a high composition of silica content have gained much attention among researchers for synthesizing mesoporous silica. To date, the only solid waste utilized for SBA-15 preparation was rice husk ash, which has been proven its efficient performance in CO₂ adsorption (Gupta et al., 2017), CO₂ chemisorption (Bhagiyalakshmi et al., 2010a) and dimethyl carbonate production (Pimprom et al., 2015). Meanwhile, oil palm industry has seen significant growth in the agricultural commodities in Southeast Asia. It has been proclaimed that roughly 7 tons of fibers, 25 tons of empty fruit bunches and 20 tons of palm kernel shells are generated for every 100 tons of raw fruit bunches processed (Iskandar et al., 2018). Palm oil fuel ash (POFA), an industrial waste acquired from the combustion of palm oil bunches and kernels at a temperature of 800-1000°C in the palm oil mill, could also be utilized as silica source substitution for synthesizing mesoporous silica. In the meantime, these POFA was subjected to open burning to reduce the solid waste disposal sites and was also disposed in the open area which was totally discouraged in the environmental conservation standpoint. Owing to the high composition of silica (57-67%), easy to find, high sustainability and eco-friendly properties in POFA (Kroehong et al., 2011), it is desirable to study the potential of POFA as an alternative sodium silicate (Na₂SiO₃) of Ni/SBA-15. Regardless on several pieces of literature declared the utilization of POFA as a promising additional cementing material or concrete (Bamaga et al., 2013), and as far we are concerned, there is no study has been done on the utilization of POFA on mesoporous catalyst preparation.

The aim of the present work is to synthesis the SBA-15 using palm oil fuel ash (POFA) as a silica source for CO₂ reforming of CH₄. An alkali fusion method was be adopted to extract silicate species from POFA for the synthesis of SBA-15, followed by impregnation of Nickel (Ni) to obtain Ni/SBA-15. The properties of the synthesized catalyts were determined using XRD, BET, SEM, TEM, TEM and FTIR-pyrrole.

Menahile, the catalytic activity of the synthesized catalysts were executed using stainless steel fixed-bed reactor.

1.2 Objectives

The objectives of this research are as follows:

1. To synthesis Ni/SBA-15 from POFA.
2. To characterize the physical and chemical properties of synthesized Ni/SBA-15.
3. To investigate and compare the catalytic activity of Ni/SBA-15 prepared from POFA on CO₂ reforming of CH₄ with conventional Ni/SBA-15.

1.3 Scopes of the study

The scopes of this research as follows:

Work scopes for objective 1

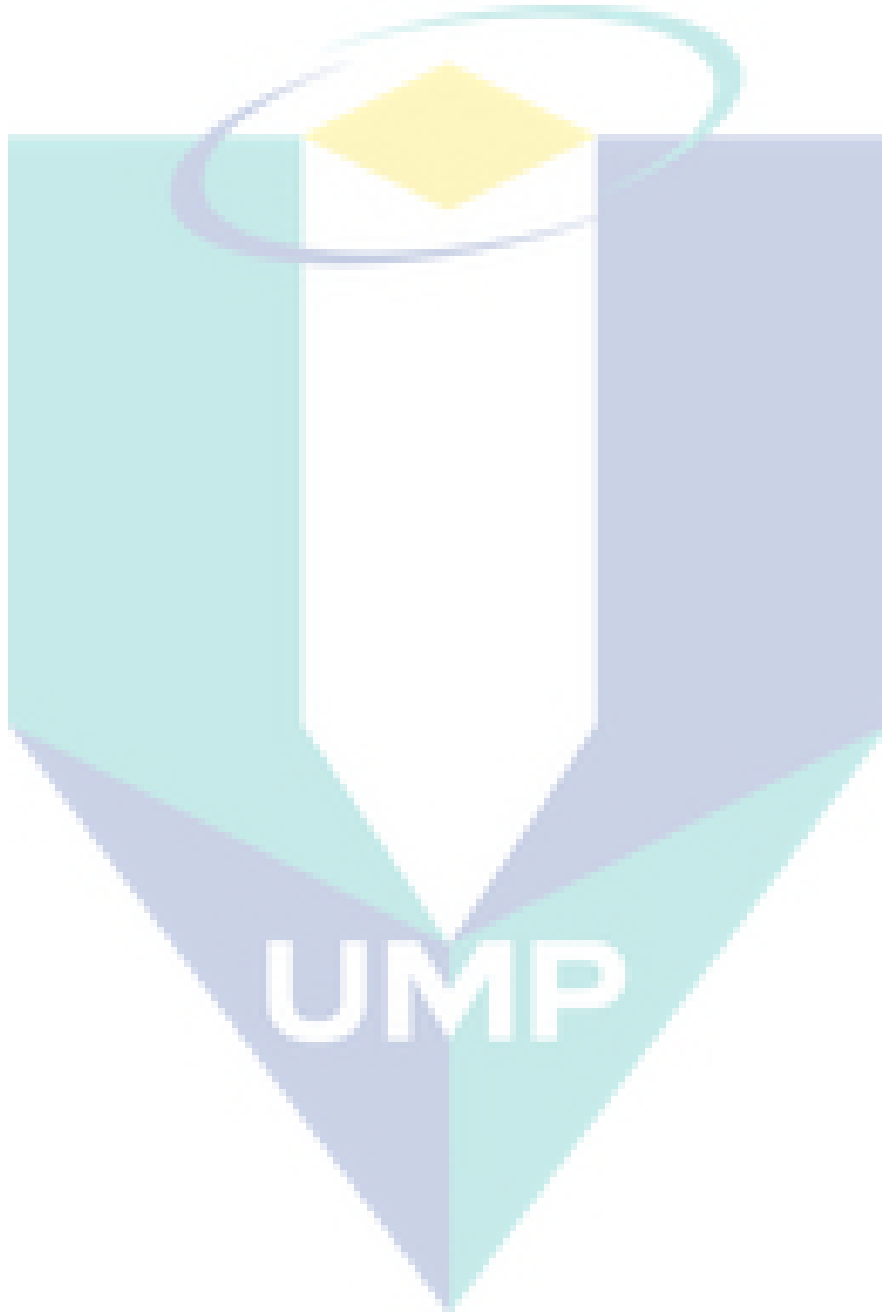
- i) Preparation of sodium silicate from palm oil fuel ash (POFA) using alkaline fusion method under several parameter including NaOH/RHA mass ratio, fusion temperature and H₂O/NaOH-fused RHA mass ratio.
- ii) Preparation of SBA-15(POFA) using sodium silicate from POFA. As comparison, commercial SBA-15 (SBA-15(C)) was prepared using commercial sodium silicate.
- iii) Preparation of Ni/SBA-15 using impregnation method various Ni loadings (1-5 wt%)

Work scopes for objective 2

Determination of the physical and chemical properties of synthesized catalyst by using x-ray diffraction (XRD), brunauer-emmett-teller (BET) specific surface area and porosity analyser, fourier transform infra-red (FTIR) spectroscopy, scanning electron microscopy equipped (SEM), transmission electron microscopy (TEM), and in-situ FTIR adsorbed Pyrrole.

Work scopes for objective 3

Investigation of the catalytic performance of Ni/SBA-15(POFA) towards CO₂ reforming of CH₄ using stainless steel fixed-bed reactor and gas chromatography (GC). The performance of synthesized catalyst was compared with SBA-15(C).



CHAPTER 2

LITERATURE REVIEW

2.1 Introduction

Global warming from increased greenhouse gases in the atmosphere is leading to a clearly, visible impacts which are detrimental effects on human beings (Lindzen, 1992). This includes spiral of worsening conditions in extreme weather events, changes in wildlife distributions health, an abundance of disease vectors, rising sea level and disappearing of glaciers and polar ice. Greenhouse gas pollution stays in the atmosphere for decades, efforts in averting devastating and irreversible impacts are required from all nations. According to the available data, global warming had increased the intensity of precipitation natural phenomenon disasters such as torrential rains and flooding, drought and wildfires, killer heat waves, disintegrating polar ice and shrinking of the snowpack (Lindzen, 1992). Global warming has also been linked to the spread of the human diseases such as malaria, yellow fever, and dengue fever. The outbreak of these diseases leads to severe and fatal illness in humans. Although weather fluctuates naturally, yet climate theory and models predict that global warming also the main contributor to some of the extreme events. It is undeniable that global warming has severe effects on many aspects of human lives (Lindzen, 1992).

Continuous efforts have been devoted to addressing the issue regarding the concern of global warming resulted of greenhouse gases, by advanced chemical reaction technologies to convert the main greenhouse gases into useful products. Among the proposed solutions, dry reforming of methane (DRM) for synthesis gas (syngas) production emerges as a promising technology compared to the industrially applied technologies for syngas production. This is due to great interest in the transformation of greenhouse gases to produce clean fuel, H₂ without net contribution to CO₂ emissions

(Vizcaíno et al., 2006). A surface reaction mechanism is proposed for defining the necessary properties of catalysts for CO₂ reforming of CH₄. As shown in Figure 2:1, the dissociative chemisorption of CH₄ occurs on the metallic centres as the metallic state of catalysts is believed to be responsible for the CH₄ activation (Yan et al., 2003). The absorption of CO₂ is supposed to take place on the surface of support since the carbon in CO₂ molecule as a Lewis acid centre tends to react with Lewis base centre of an oxide. Figure 2-1 shows the proposed mechanism for CO₂ reforming of CH₄ in which the presence of metal particles as catalyst and catalyst support will enhance the process.

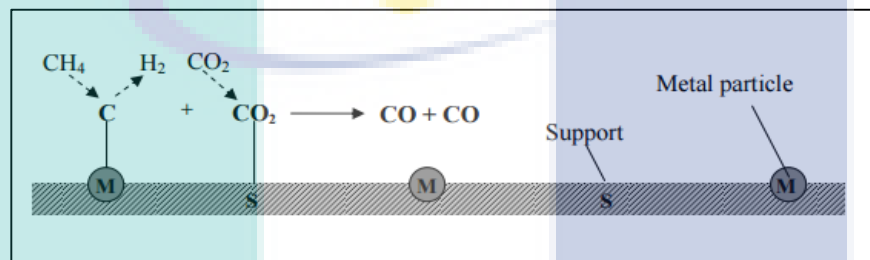


Figure 2:1 Proposed surface mechanism for CO₂ reforming of CH₄

Source: Yan et al. (2003)

The heterogeneous catalyst for DRM generally consists of support materials and promoters. mesoporous catalytic supports have many advantages to be used in the catalytic reaction. In comparison with the other regular mesoporous materials, Santa Barbara Amorphous (SBA-15) can be prepared in larger pores, resulting in a more stable structure (Ye et al., 2011). In addition, SBA-15 poses high hydrothermal stability and shows high activity due to its high surface area and huge pore volume (Razali, 2009); (Amin et al., 2012; Ye et al., 2011). Thus, SBA-15 is the catalyst support in this research.

It is well known that the cost for the large-scale manufacture of SBA-15 is high, owing to the cost of both templates and silica source. Therefore, the utilization of waste materials as alternative silica source would minimize the cost of production. POFA consists of high amount of silica and has a great potential to be used as an alternative silica source to synthesis SBA-15. Since palm oil industry is the major agro-industries in Malaysia that generating a huge amount of POFA waste as high as 4 million tons compared with 3 million tons produced in 2007 (Khan et al., 2015). Thus, the use of POFA as a silica source provides a solution to the economic disposal of waste generated from palm oil factories, and indirectly reduce the cost of SBA-15 production.

Since SBA-15 is chosen as the most promising catalyst support for CO₂ reforming in this study, lacks of acidity characteristics in purely siliceous SBA-15 will hinder its ideal capabilities as a catalyst. Modification and functionalization of SBA-15 could enhance and optimize its catalytic activity. Although noble metals demonstrate highest catalytic stability, the Ni-based catalysts appear to be promising for future processes in industrial scale. Due to its high catalytic activity and low cost, the nickel catalyst is considered as one kind of the promising catalyst for steam reforming. They found to have promising catalytic performance in term of conversion and selectivity for dry reforming of methane (Vizcaíno et al., 2006). The high cost of noble metals makes them a less than ideal choice (Razali, 2009). Moreover, smaller Ni particles have a higher stability to suppress the carbon deposition (Cai et al., 2014); (Vizcaíno et al., 2006). Therefore, Ni is chosen as the metal catalysts in this study for the synthesis of Ni/SBA-15.

2.2 Carbon cycle

2.2.1 Carbon cycle, Global Warming, and Greenhouse Gases

Carbon is being stored not only in the atmosphere but also in the land surface, vegetation and but also in the ocean. Carbon cycle happens when enormous quantities of carbon are exchanged between the atmosphere, ocean and the land surface (Folger, 2009). High amount of carbon is contributed by human activities, in which mainly as CO₂ to the carbon cycle. In fact, over half of CO₂ comes from energy sector activities which in turn results in CO₂ as the major human-produced greenhouse gas. The major contributors to the increased concentration of CO₂ in the atmosphere are a power station and the petrochemical industries. CO₂, one of the greenhouse gases increases drastically leads to the heat-trapping capacity of the earth's atmosphere being enhanced (Lindzen, 1992). During the heating trapping process, the air currents will carry the heat upwards and then the surface is cooled by the air currents too which form an air circulation. Determining the temperature of the earth is primary importance as a consequence of this (Lindzen, 1992). Carbon dioxide (CO₂), methane (CH₄) are the main composition of greenhouse gases including, water vapour (H₂O), ozone (O₃), nitrous oxide (N₂O), chlorofluorocarbons (CFCs) (Ahmed, 2011) .Among the greenhouse gases, with 72% of the total emitted greenhouse gas into the atmosphere is CO₂. This indicates that the CO₂ is the largest contributor and the fastest growing emitted component. Thus, this results in the global warming (Sanglimsuwan, 2011). The concentration of CO₂ is expected to

continue rising in the future due to the industrial involution nowadays. According to (Wang et al., 2012), the concentration of CO₂ in the atmosphere can reach up to 570ppm by the ned of the century. One the other hand, CH₄ comprises 18% of the total greenhouse gas emitted to the atmosphere (Sanglimsuwan, 2011). Carbon released from human activities is consumed not fast enough by the oceans, vegetation, and soil, therefore, the carbon is trapped and accumulated in the atmosphere (Folger, 2009). In order to combat the rising carbon concentration in the atmosphere, therefore, it is essential that we figure out alternatives to reduce the CO₂ emissions to the atmosphere (Watson et al., 2011). Global temperatures are expected to rise between 1.4 and 5.8 °C by 2100 and sea level could also rise between 0.09 and 0.88 meters compared to 1990 levels, without action to reduce greenhouse gas emissions (Watson et al., 2011). The carbon cycle around the atmosphere, sea and land is shown in Figure 2:2.

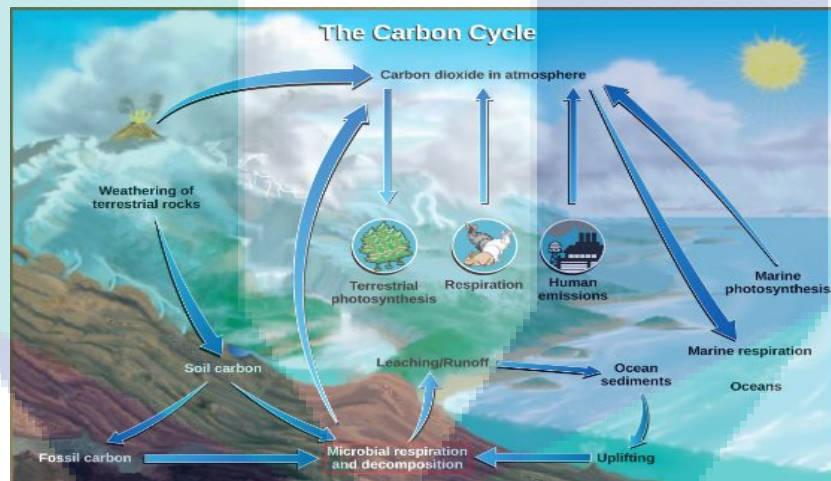


Figure 2:2 The Carbon Cycle

Source: Prentice (2015)

2.2.2 Previous effort options to decrease CO₂ emission

As far as we are concern, the process of continuation releasing of energy-related CO₂ into the atmosphere pose a serious risk when the current energy source is predominantly dependent on fossil fuels .Thus, alternatives sources of energy, new strategies or new technologies that could reduce the migration of CO₂ into the atmosphere should be developed (Ahmed, 2011). A number of options that can be used in order to reduce the CO₂ release are discussed clearly below (Ahmed, 2011).

Clean coal technologies are emerged as one of the alternatives to reduce the CO₂ emission that will lead to global warming. Urea production is one of the ways included in this technology. At present, urea is generated from inexpensive natural gas during the manufacturing process, which is produced from ammonia and carbon dioxide. The available CO₂ may be insufficient in view of the balance between ammonia and off-gas CO₂ when urea is synthesized with natural gas as a raw material (Folger, 2009). In conjugation of this case, CO₂ is recovered from the exhaust gas of the steam reformer to supply it for urea synthesis to adjust the ammonia-CO₂ balance. Therefore, large quantities of urea can be produced. There are few plants that match with the purpose, such as Mitsubishi Heavy Industries plant, Malaysia PETRONAS Fertilizer Sdn. Bhd (Folger, 2009).

On the other hand, methanol is now also manufactured using natural gas as the feedstock. The H₂: CO ratio used for methanol production is 3:1 by steam reforming process. However, the best H₂: CO ratio for methanol synthesis is 2:1 (Gabriele et al., 2013). To maximize the output of methanol, the CO₂ emitted from the process should be recovered from steam reformer flue gas to allow the addition amount of CO₂ into the process (Lanjekar et al., 2011). At Saudi Arabian methanol plant, active planning for CO₂ addition is underway to improve the production capacity (Gabriele et al., 2013). Figure 2:3 shows the general process for methanol production with natural gas as the feedstock, in which the CO₂ produced from the steam reformer are recovered back in order to optimize the H₂:CO ratio for methanol synthesis, thereby enhancing methanol production (Gabriele et al., 2013); (Lanjekar et al., 2011).

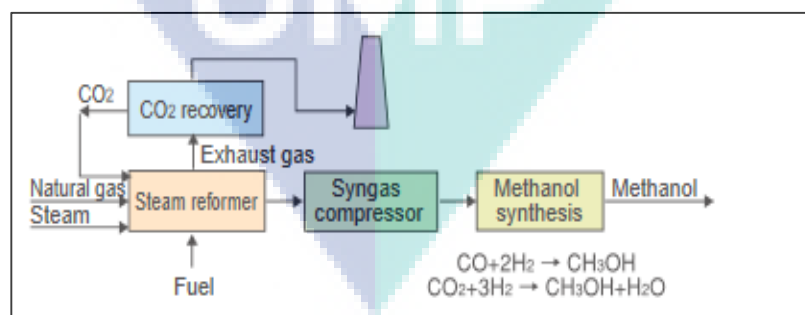


Figure 2:3 CO₂ recovery from flue gas for enhanced methanol production. Sources: Gabriele et al. (2013; Lanjekar et al. (2011)

In addition, deforestation in tropical countries accounts for about 15% of global warming pollution. Due to vast areas are being cleared for agriculture expansion, tropical

forests become a net source of carbon emissions. This results in the only small amount of carbon being absorbed each year because the remaining forests grow slowly. Nations should reduce the net global warming emission from tropical forests 50% by 2020, and bring them to zero by 2030, in order to help mitigate the worst effects of climate change (Ellis & Porter-Bolland, 2008). Other than providing oxygen for us to breathe, tropical forests also take CO₂ out of the atmosphere and store much more carbon than forests in temperate (Elias & Lininger, 2010). Trees convert carbon dioxide, water and sunlight into oxygen, by locking up carbon in their trunks and branches during photosynthesis process (Elias & Lininger, 2010). The fastest and the most cost-effective way to reduce carbon dioxide emission from tropical forests are reducing deforestation and forest degradation (Verchot et al., 2006). These two activities have big impacts on climate change if being acted quickly (Niles et al., 2002). Previous effort on reducing tropical deforestation and replantation will guarantee Earth's ability to remove carbon from the atmosphere and avoid the worst effects of global warming (Elias & Lininger, 2010).

The market for climate-friendly services and products is growing rapidly, from new renewable energy systems to energy efficient products. A more systematic approach comes from the field of 'design for sustainability', which includes life cycle design and environmentally conscious design and manufacturing. This new approach considers environmental aspects at all stages of development to create products with the lowest environmental impact throughout the product life cycle (Talukdar et al., 2011). Hybrid or electric cars are the marvelous creation to improve the energy efficiency and decrease CO₂ emission. Solar and geothermal energy are renewable energy that emits little or no CO₂. Same goes to biomass, wind and wave energy, they also can be sources to generate electricity (Wang et al., 2012).

2.2.3 Catalytic reforming of methane with CO₂

Production of synthesis gas from CH₄ and CO₂ was first suggested in 1928 by Fischer and Tropsch (Lu & Lee, 2007) due to their great interest in an alternative process to coal gasification. The catalytic reforming of methane gained the great attention of researchers (Ashcroft et al., 1991) because it consumes two greenhouse gases simultaneously, CO₂ and CH₄. This process is especially preferable for hydroformylation reactions (Oxo synthesis) of alkenes to aldehydes and Fischer-Tropsch reactions of long chain alkanes as it produces a syngas with an H₂/CO ratio of equal to or less than unity,

which is (Mette et al., 2014; Wang & Lu, 1996). Catalytic reforming of methane with CO₂ also known as dry reforming of methane (DRM). Syngas produced can be used in a variety of downstream processes such as hydroformylation processes, Fischer-Tropsch synthesis and methanol production (Amin et al., 2012). Through dry reforming, a high CO selectivity, and a more suitable H₂/CO ratio will be obtained (Amin et al., 2012). This process is an energy consumer to eliminate CH₄ and CO₂ that is subsequently beneficial in term of economical and also environmental (Chawl et al., 2013). A higher purity of CO can also be made other than CO₂ is being consumed (Wurzell et al., 2000).

Although steam reforming of methane (SRM) was the dominant commercial method employed to produce syngas, yet DRM is proposed to catalytically reform methane with carbon dioxide due to the limitations posed by SRM (Ruckenstein & Hu, 1995). The reaction limitations listed below limits the large-scale commercial use of SRM.

- High energy consumption because of the highly endothermic property of the reaction.
- Poor selectivity for CO (Ruckenstein & Hu, 1995)

Moreover, the partial oxidation is another reaction used to convert methane into syngas. Partial oxidation is a mildly exothermic reaction and has fewer reaction limitations than SRM. However, it process faces a big difficulty to remove the huge amount of heat generated in the reactor after the methane conversion (Ruckenstein & Hu, 1995).

In comparison among the several ways to produce syngas, DRM is chosen as the most promising process as it offers the advantage in that it does not only produce syngas with controlled H₂/CO ratio but also mitigates the formation of particulate carbon deposition. The DRM yields syngas with a lower ratio of H₂/CO, i.e.: 1: 1 for a complete conversion. This ratio is preferable for the synthesis of higher carbons via Fischer-Tropsch. In general, the DRM may be the most effective process whenever carbon dioxide is a by-product which available for utilization. A catalyst is needed for the DRM reaction in order to speed up the process and gain a satisfactory reaction rate. DRM is first studied by Fisher and Tropsch over a number of base metal catalysts. The reaction

is thermodynamically favoured above 913 K, and it is more endothermic than SRM. Figure 2:4 shows the schematic diagram for CO₂ reforming of CH₄.

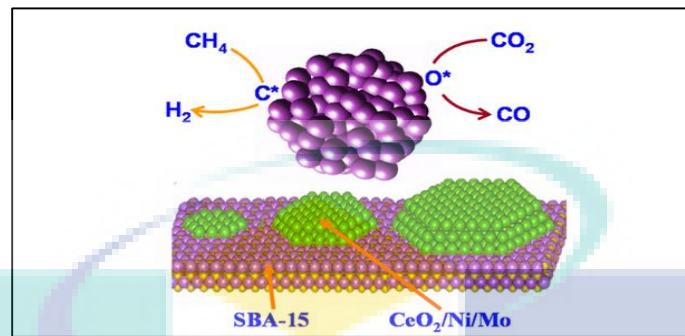


Figure 2:4 Schematic Diagram of CO₂ reforming of Methane
Source: Huang et al. (2011)

Furthermore, the DRM can be considered as alternatives to produce energy by storing solar energy or nuclear energy through a chemical energy transmission energy system (CETS). From Figure 2:5, it can be seen that the endothermic reforming is carried out when there is the presence of solar energy or nuclear energy. The products formed will be stored until energy is required. Then, an exothermic reaction will take place to release energy.

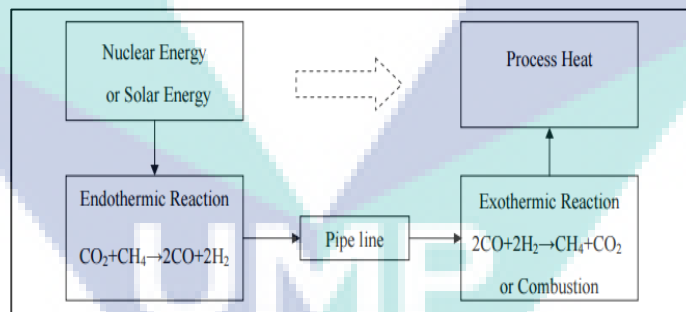


Figure 2:5 The Chemical Energy Transmission System (CETS)
Source: Zhang (2008)

2.3 Syngas

Syngas is an important feedstock for the production of a number of materials such as methanol, ammonia, diesel fuels or synthetic gasoline (Fischer-Tropsch process) in catalytic processes (Navarro et al., 2013). Furthermore, syngas can be used directly as H₂ source or being burned, e.g. in gas turbines, to produce electricity and heat. Syngas is used to produce aldehydes for the Hydroformylation reactions (oxo synthesis) of alkenes,

(Navarro et al., 2013). The H₂/CO ratio can be adjusted by the water gas shift reaction depends on the H₂/CO ratio required. Different syngas synthesis route, will result in different H₂/CO ratios. Figure 2:6 reveals the several usages of syngas.

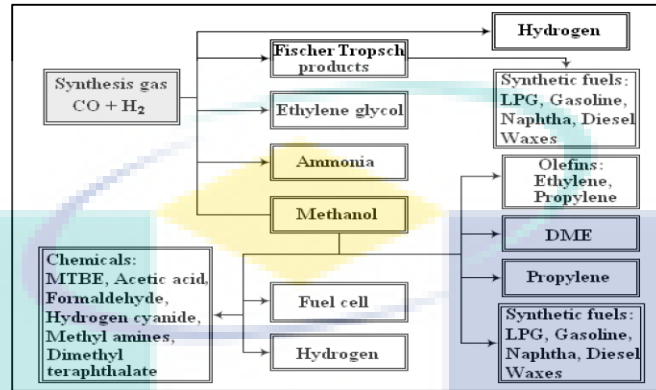


Figure 2:6 Main usage areas of syngas

Source: York et al. (2007)

There are mainly four synthesis routes to produce syngas which is clearly shown Figure 2:7. Commercially used methods for syngas production are especially the steam reforming of natural gas and to some extent the gasification of coal (Choudhary & Choudhary, 2008). However, these processes required high energy needs and high consumption of fossil fuels. The high energy needs can be supplied by the combustion of additional fossil fuels. Partial oxidation of methane (Pompeo et al.) or the dry reforming of methane (DRM) appeared as the alternative routes (Gadalla & Bower, 1988). In contrast to the commercial process, the POM and DRM processes are required lesser energy, with the former is an exothermic reaction and the latter one is capable of transforming CO₂ directly, though, it is highly endothermic as well. Table 2:1 summarizes the reaction equations and heat of reaction in each synthesis routes.

Table 2:1 Processes Producing Syngas

Process	Reaction Equation	ΔH_{298K}^0
Steam Reforming	$CH_4 + H_2O \leftrightarrow CO + 3H_2$	206
Partial Oxidation	$CH_4 + 0.5 \leftrightarrow CO + 2H_2$	-36
Dry Reforming	$CH_4 + CO_2 \leftrightarrow 2CO + 2H_2$	247
Autothermal Reforming	$CH_4 + 2O_2 \leftrightarrow CO_2 + 2H_2O$	-802
	(Methane in excess)	
	$CH_4 + CO_2 \leftrightarrow 2CO + 2H_2$	247
	$CH_4 + H_2O \leftrightarrow CO + 3H_2$	206

Source: (Choudhary & Choudhary, 2008)

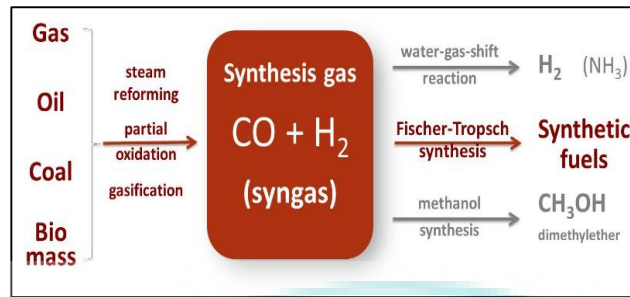


Figure 2:7 Synthesis Routes of Producing Syngas

Source: Loosdrecht & Niemantsverdriet (2013)

2.4 Waste materials as silica source

Malaysia is rich in natural sources such as rice husk, sugarcane bagasse, fly ash and POFA. These waste materials in large quantities can create a serious environmental problem. Hence, there is a need to adopt a proper strategy to reduce the waste. Recently, the studies had been focusing on the utilization of these waste and the potential of these waste to be utilized in the researches will be discussed as below.

Rice milling generates a by-product known as rice husk ash (RHA) (Habeeb & Mahmud, 2010a). According to (Nagrle et al., 2012), about 220kg (22%) of the husk is produced for every 1000kg of paddy milled and when the husk is burnt in the boiler, about 55kg (25%) of the RHA is generated and when the husk is burnt in the boiler, about 55kg (25%) of RHA is generated (Nagrle et al., 2012). Rice husk is an agriculture residue accounts for 20% of the 649.7 million tonnes of rice produced annually worldwide (Chandrasekhar et al., 2006); (Habeeb & Mahmud, 2010b). The chemical composition of rice husk will be affected by the differences in the geographical conditions type of paddy, crop year and climate (Chandrasekhar et al., 2006). Ash with silica mainly in amorphous can be obtained from burning the husk under controlled temperature below 800°C (Chandrasekhar et al., 2006). Due to its high silicon content, the rice husk has become a source for preparation of elementary silicon, silicon carbide and silicon nitride (Hunt et al., 1984). Most of the metallic impurities in the RHA can be removed by leaching rice husks with a solution of HCl , HNO_3 , H_2SO_4 before treatment proved and subsequently producing ash-silica completely white in colour with the high specific surface area (Hunt et al., 1984). The SiO_2 composition in rice rush can reach from 85-98% after burning out (Della et al., 2002). The chemical composition of RHA after burning out is summarized in Table 2:2.

Table 2:2 Chemical Properties of RHA after burning out

Chemical Composition	%
Silicon Dioxide (SiO ₂)	88.32
Aluminium Oxide (Al ₂ O ₃)	0.46
Ferric Oxide (Fe ₂ O ₃)	0.67
Calcium Oxide (CaO)	0.67
Sodium Oxide (Na ₂ O ₃)	0.12
Magnesium Oxide (MgO)	0.44
Potassium oxide (K ₂ O)	2.91
Sulphur Oxide (SO ₃)	0.33
Loss of Ignition (LOI)	5.81

Source: Habeeb & Mahmud (2010a)

Sugarcane bagasse is another most common agricultural wastes and valuable biomass by-products in sugar milling, which being utilized for its high silica content. The high percentage silica content from bagasse ash was used as a silica source for sodium silicate solution. Bagasse is the main by-product of the sugar extraction from the sugarcane (Kuprianova et al., 2006). In another word, bagasse is a cellular fibre remaining after the extraction of the sugar-bearing juice from sugarcane. Bagasse ash is one of the biomass sources of energy and it is well-known that bagasse ash is an alternative source of energy with high silica content. This sugarcane bagasse ash which is obtained after the burning of sugarcane bagasse to produce energy and steam for power is a solid waste that is not biodegradable. Chemical properties of sugarcane bagasse after acid treatment with oxygen is shown in Table 2:3.

Table 2:3 Chemical Properties of Sugarcane Bagasse after Acid Treatment with Oxygen

Chemical Composition	%
Silicon Dioxide (SiO ₂)	89.04
Aluminium Oxide (Al ₂ O ₃)	0.79
Ferric Oxide (Fe ₂ O ₃)	1.97
Calcium Oxide (CaO)	2.55
Phosphorus Oxide (P ₂ O ₃)	1.69
Manganese oxide (Mn ₂ O ₃)	0.15
Potassium oxide (K ₂ O)	2.13
Sulphur Oxide (SO ₃)	0.33
Other	0.79

Source: Worathanakul et al. (2009)

Approximately 80 million tons of fly ash are produced from the coal-fired plants each year. Fly- ash can be defined as the end residue from the combustion of sub-

bituminous coal in the furnace of thermal power plants which consists of mineral constituents of coal which are not fully burnt. The fly ash, as a fine particulate residue is removed by the dust-collection system from the combustion gases before they are discharged into the atmosphere. Fly ash is a fine-grained material consisting mostly of spherical particles. Some ashes also contain irregular or angular particles. The physical properties of fly ash vary widely depending on the coal type, boiler type, and ash content in coal, combustion method, and collector setup. Fly-ash particles are empty spheres (cenospheres) filled with smaller amorphous particles and crystals (plerospheres). In general, fly-ash has a low bulk density (1.01–1.43 g/cm³), hydraulic conductivity and specific gravity (1.6–3.1 g/cm³) (Pichtel & Hayes, 1990; Torrey, 1978; Cheremisinoff, 1988). Mean particle densities for non-magnetic and magnetic particles are 2.7 and 3.4 g cm³, respectively, while the moisture retention ranges from 6.1% at 15 bars to 13.4% at 1/3 bar (Dlugi., 1983). Table 2:4 lists out the chemical composition of fly ash.

Table 2:4 Chemical Composition of Fly Ash

Chemical Composition	%
Silicon Dioxide (SiO ₂)	50.6
Aluminium Oxide (Al ₂ O ₃)	25.5
Ferric Oxide (Fe ₂ O ₃)	7.9
Calcium Oxide (CaO)	9.1
Magnesium Oxide (MgO)	2.1
Sodium Oxide (Na ₂ O)	0.43
Potassium oxide (K ₂ O)	0.55
Sulphur Oxide (SO ₃)	0.4
Other	3.42

Source: El-Mogazi et al. (1988)

POFA is also a waste that rich in silica source in our country. POFA is a by-product from the combustion of palm oil shells and palm oil bunches in palm oil mill boiler to generate electricity in biomass thermal power plant (Sata et al., 2004). Physical characteristics of the as-received and ground POFA shows that visual appearance of the raw ash was characterized by dark spongy and porous structure. Main constituents of the raw ash include hard but light weight honeycombed impurities, and irregular shape and cellular textures. However, POFA beneficiation through sieving and the two-stage pulverization processes revealed that the ash was having the grayish appearance, after sieving through the 150. According to the studies done by (Kroehong et al., 2011) and (Yeung et al., 2005), the surface of the POFA is porous and spongy. The collection of ash was done at the foot of the flue tower where all the fine ashes are trapped while escaping

from the burning chambers of the boiler. After the collection, all the ashes were sieved through a sieve in order to remove the bigger size ash particles and foreign materials. After burning, the resulting ash, known as POFA, is generally disposed of in open fields, thus creating environmental and health problems (Tonnyapas et al., 2006). POFA has been identified as a good pozzolanic material. This kind of ashes has a great potential to develop as geopolymer composites due to its high quantities of silica (Si) which (Zarina et al., 2013).

POFA is greyish in colour, but will become dark with the increasing proportions of unburnt carbon (Jamo & Abdu, 2015). The ground POFA was shown to be amorphous in structure after the morphological (Oyeleke et al., 2011). In the biomass boiler mills and thermal power plants, the typical inlet temperature utilized ranges from 800 to 1000°C (Wunchock et al., 2011). At control temperature lower than 700°C, high-grade amorphous silica may be produced when biomass wastes are burnt. (Warid & Khairunisa, 2009). The physical properties of the as-received and ground POFA are presented in Table 2:5 whereas Table 2:6 presents the chemical composition of POFA. For Table 2:7, a comparison on the four waste materials discussed above is made and summarized.

Table 2:5 Physical Characteristics of the Raw and Processed POFA

Physical properties	Appearance before ignition	Appearance after ignition	Texture	Shape
Raw POFA	dark spongy	porous, greyish	hard, gritty, light, cellular	Irregular
Ground POFA	greyish, powdery	brownish	Powdery	Round

Source: (Oyeleke et al., 2011)

Table 2:6 Chemical Composition of POFA

Chemical Composition	%
Silicon Dioxide (SiO ₂)	82.07
Aluminium Oxide (Al ₂ O ₃)	6.04
Ferric Oxide (Fe ₂ O ₃)	2.70
Calcium Oxide (CaO)	5.11
Magnesium Oxide (MgO)	2.28
Sodium Oxide (Na ₂ O)	1.34
Potassium oxide (K ₂ O)	2.90
Sulphur Oxide (SO ₃)	2.20
Loss of Ignition (LOI)	5.30

Source: Yahaya et al. (2015)



Figure 2:8 Incinerator producing POFA

Source: Yahaya et al. (2015)



Figure 2:9 POFA dumped as waste

Source: Yahaya et al. (2015)

Table 2:7 Types of Waste Materials as Silica Source

Waste Material	Description	Source
Rice Hush Ash	Consists of 90-98% silica (after complete combustion) A by-product of the rice milling industry. Has high amorphous silica content	(Della et al., 2002); (Selvakumar et al., 2014); (Mittal, 1997); (Bhagiyalakshmi et al., 2010)
Sugarcane bagasse Ash	Consists of > 89% silica. A by-product in sugar milling.	(Arumugam & Ponnusami, 2014)
Fly Ash	Consists of 40-60% silica for sub-bituminous type. The end residue from the combustion of pulverized bituminous or sub-bituminous coal (lignite) in the furnace of thermal power plants.	(Kumar et al., 2013); (Faizul et al., 2012)
Palm Oil Fuel Ash (POFA)	Consists of 82 % silica. The by-product from the combustion of palm oil shells and palm oil bunches to generate electricity in biomass thermal power plant. Has crystalline structure with porous cellular structure and irregular-shaped particles. Greyish in color	(Chen et al., 2010) (Khan et al., 2015); (Du et al., 2008); (Safiuddin et al., 2011); (Jamo & Abdu, 2015)

In short, fly ash which is the end residue from the combustion of pulverized bituminous or sub-bituminous coal consists of the lowest silica content as compared to rice husk ash, sugarcane bagasse ash and palm oil fuel ash (POFA). If comparing in terms of availability, palm oil fuel ash (POFA), the by-product from the combustion of palm oil shells and palm oil bunches can be considered as available abundantly in Malaysia as compared to fly ash and sugarcane bagasse ash. Thus, POFA is chosen as the silica source for the catalyst preparation.

2.5 Previous studies on CO₂ reforming catalysts

According to previous studies, there are several types of noble metals that have been used in the dry reforming reaction such as rhodium, palladium, iridium, ruthenium and platinum (Ruckenstein & Hu, 1995). More or less catalytic activity shown by these noble metals towards the reaction (Ruckenstein & Hu, 1995). Due to the reduced sensitivity to carbon deposition DRM on noble metal catalysts exhibits not only very high stability but also better activity (Ruckenstein & Hu, 1995). Among the noble metals, highest activity for DRM is shown by Ruthenium and rhodium (Rezaei et al., 2006). Although Ruthenium can perform with high reforming activity with its low carbon growth rates, the availability of ruthenium production is too low to have a major impact, which is estimated at 4 tonnes annually (Rostrupielsen & Hansen, 1993). Since the DRM reaction is endothermic, therefore high operation temperature is required to stimulate metal sintering and deactivation caused by carbon deposition (Ruckenstein & Hu, 1995). Compared to non-noble metal based catalysts, noble-metal-based catalysts can provide operations with lower carbon deposition. However, it is more practical to develop an active nickel-based catalyst that resists the coke formation rather than using the high cost and limited availability of noble metals (Zhang et al., 2008; Zhang & Verykios, 1994).

There are also non-noble metals which have been used previously such as nickel and cobalt. Supported nickel catalysts constitute materials often used due to their activity and low cost. The main challenge faced when nickel is being used in the natural gas reforming is the high carbon formation and the sintering of the metallic phase. This will, in turn, create instability of the catalyst. Indeed, the active site of the catalyst can be stabilized by the addition of alkali modifiers such as Na, K, Li (Pompeo et al., 2005). There have been different catalysts employed for dry reforming of CO₂. However, Ni-based catalysts are considered as the most promising catalyst to be used as they exhibit

cost-effective, readily available. From the Table 2:8, it is clearly shown that Ni is not the most active metals to be used yet it is the widest used metal from this set. This is because Ni is more prone to deactivation by, e.g., carbon formation or oxidation.

Table 2:8 Relative activities for steam reforming of methane, T = 550°C, S/C = 4, P = 1 bar

Catalyst metal content (wt%)	Relative Rate
Ni (16)	1.0
Ru (1.4)	2.1
Rh (1.1)	1.9
Pd (1.2)	0.4
Ir (0.9)	1.1
Pt (0.9)	0.5

Source: Rostrup-Nielson et al. (1993)

The activity of the catalyst is closely related to the metal surface area (i.e., the number of active sites). This implies that higher dispersion of the metal particles will result in a higher catalytic activity. Ni metal particles of 20–50 nm of 2–5%, are the common catalyst dispersion. (Rostrupnielsen & Hansen, 1993). When the Ni content reached the optimum beyond, an increase in Ni-content does not produce any increase in activity, usually around 15–20 wt. % (depending on the support structure and surface). The dispersion or utilization of the nickel tends to decrease with increasing nickel content although the nickel surface area is generally increased with higher loadings. Hence, the activity will not increase any further. The Ni particle size seems to be an important factor for the activity of reforming catalysts. Usually, the smaller particles can improve the catalyst activity by providing a larger surface for reaction. On the other hand, larger crystallites of nickel will cause catalyst deactivation by catalyst deactivation. (Christensena et al., 2006). Based on the Table 2:9, comparison is made to reveal the advantages and the disadvantages of the most common loading to be used in CO₂ reforming of CH₄.

Table 2:9 Types of Metal Loading

Types of Metal	Advantages	Disadvantages	Source
Nickel (Ni)	High catalytic activity Remarkable capability in C-C bond cleavage Low cost Readily available Cost effective High mechanical strength	Easily deactivated because of carbon deposition Active metal species sintering	(Estephane et al., 2015); (Chawl et al., 2013); (Amin et al., 2012); (Yang et al., 2015)

Copper (Cu)	Stable Strong inhibitor of coke formation Highly active and selective	Costly	(Chen et al., 2009); (Vizcaíno et al., 2006)
Cobalt (Co)	Shows good performance in the production of syngas via methane dry reforming	Lead to the disappearance of long range order SBA-15. Decrease surface area of SBA-15.	(Rahmat et al., 2010)
Ruthenium (Ru), Rhodium (Rh), Palladium (Pd)	Highly resistant to carbon deposition High catalytic stability.	High cost	(Estephane et al., 2015)
Aluminium (Al)	More stable than pure SBA-15 in which the pore spacing, wall thickness still remains the same.	Specific surface area and pore volume decrease in basic medium treatment.	(Rahmat et al., 2010)

In summary, Nickel (Ni) possess the most advantages among the several metal being discussed above with its readily availability at relative lower price. Besides, its capability of performing a high catalytic activity will be a great advantage when performing CO₂ reforming of CH₄. The rest of the metals discussed such as copper (Cu), cobalt (Co), aluminium (Al) mostly are high in price with limited advantages. By considering the overall performance, Nickel (Ni) is chosen as the noble metal used in dry reforming reaction.

2.6 Mesoporous materials as catalytic support

It is widely known that the catalytic performance is greatly affected by the active surface area and the acid-base property of the catalyst support. The adsorption and dissociation of CO₂ involved in the reaction and the performance can be improved by a basic support since the CO₂ gas is an acid gas (Amin et al., 2012). Deactivation happened in the process is a major problem encountered due to the carbon deposition on the surface, leading to blockage of reactor tubes (Amin et al., 2012). Other than coke formation, the loss of catalytic activity can also be affected by metal sintering. In this case, catalyst support will play an important role in participating in the catalytic reactivity and acting on coke resistance of the metal particles. According to Amin et al (2012), catalytic activity and stability are greatly influenced by support type. Generally, the role of the

support is used to provide support for the metal catalyst materials, in order to obtain a stable and high active surface area.

Amin *et al* (2012) studied on the effect of support material towards CO₂ reforming of methane. In this study, they used different types of support which are SBA-15, KIT-6, MCM-41 and SBA-15. They found that the activity of the catalyst influenced by the type of support material and the activity followed the order of Ni/SBA-15 > Ni/KIT-6 > Ni/Al₂O₃ > Ni/MCM-41. This activity sequence is correlated strongly with the surface area and pore diameter of these materials with the degree of CH₄ and CO₂ conversions observed. The Ni/ SBA-15 which exhibited excellent catalytic performance in term of long-term stability as well as catalytic activity is the best among the mesoporous materials (Amin et al., 2012). In fact, the activity of the Ni/SBA-15 towards the degree of conversion of both CO₂ and CH₄ is much correlated to the surface area and the pore distribution (Amin et al., 2012). The Ni/SBA-15 catalyst can perform excellent catalytic performance with its more active in terms of CH₄ and CO₂ conversion than all of the other materials due to an obvious increase in the pore size, pore volume but decrease in BET surface after the Ni being introduced (Amin et al., 2012). A CH₄ conversions between 84.5 and 85.1 % and a CO₂ conversion of ~92.4 % can be performed by this type of catalyst (Amin et al., 2012). The textural properties of different samples are provided as the table below in which the catalytic performance increasing with decreasing surface area and increasing pore diameter. The Ni/SBA-15 catalyst is producing the synthesis gas with the highest H₂/CO ratios of 0.97 (Amin et al., 2012). The ability of Ni/SBA-15 catalyst to produce this high H₂/CO ratio can be explained due to reduced water gas shift reaction occurred (Amin et al., 2012). This situation takes place due to the much more rapid conversion of CO₂ on Ni/SBA-15.

Furthermore, the rate of carbon deposition on the catalysts was as follows: Ni/KIT-6 (0.0002) < Ni/ MCM-41 (0.0003) < Ni/SBA-15 (0.0005) (Amin et al., 2012). This also proves that The Ni/KIT-6 catalyst poses the lowest carbon deposition rate if compared to others two. Although MCM-41 has the lowest carbon deposition rate, yet it is very unstable at high temperatures because of the thermal deterioration (Amin et al., 2012). Mesoporous silica SBA-15 has attracted significant attention in catalysis due to its highly ordered hexagonal structure with narrow pore size distribution, thick pore wall,

and high surface areas. In comparison with straight pores in MCM-41, the highly ordered two-dimensional hexagonal structure of SBA-15 is found to be much better as a support.

In addition, supports have many functions but the most important are to maintain a stable physical surface, especially at high reaction temperatures. Therefore, the support itself must resist to thermal transformation at high temperatures, which means catalyst support must have high melting points. The melting points of catalyst supports that are most often studied in the CO₂ reforming of CH₄ are tabulated in Table 2:10. Al₂O₃ and SiO₂ are two of the most often investigated catalyst supports with the high specific surface area. MgO and CaO are studied due to their high melting points which favour stable catalyst surfaces at high reaction temperatures. Also, their basicity is believed to suppress carbon formation by promoting the activation of CO₂ (Zhang & Verkios, 1994). Even though same active metals and supports are selected to make a catalyst, the performances of catalysts may be very different since catalyst performances are easily affected by a variety of other factors other than composition, such as preparation methods, thermal treatments, activation procedures, content of active components and precursors of active components.

Table 2:10 Melting Point of Metal Oxides as Catalyst Support

Support	Melting Point (°C)
Al ₂ O ₃	2318
SiO ₂	1973
MgO	3073
CaO	2853
TiO ₂	2113
ZrO ₂	2988
CeO ₂	2873
La ₂ O ₃	2588

Source: Richardson (1989)

In summary, the advantages of good structural stability and the unique pore structural properties of SBA-15 make this a promising catalytic support material for Ni for use in the dry reforming of methane. The comparison between the catalytic supports is being summarized in Table 2:11. In summary, the advantages of good structural stability and the unique pore structural properties of SBA-15 make this a promising catalytic support material for Ni for use in the dry reforming of methane. The schematic diagram of SBA-15 is shown in Figure 2:10.

Table 2:11 Types of Catalytic Support

Types of Catalytic Support	Example	Advantages	Disadvantages	Author
Mesoporous	SBA-15 FSM-16 M41S family	Well-ordered hexagonal array structure. High surface area High stability Highly uniform pore distribution and tunable pore size. 5 High adsorption capacity	Difficulty of maintaining the mesostructured of the functionalized silica materials. Lack of pH stability.	(Amin et al., 2012); (He et al., 2015); (Sonwane & Li, 2005); (Cheng, 2013); (Razali, 2009)
Metal Oxides	Al ₂ O ₃ MgO	High mechanical strength. High surface area. High catalytic activity. Long-term catalytic stability.	Expensive Serious coking on the forming catalyst.	(Han et al., 2013); (Roh et al., 2002); (Yang et al., 2015)
Zeolite	ZSM-5	Well-defined structure The properties of the active metal can be accurately controlled.	The great sensitivity of zeolites to deactivation. Inefficient Expensive	(Smith, 1963)

Figure 2:10 Schematic diagram of SBA-15

Source: Albayati & Doyle (2014)



CHAPTER 3

METHODOLOGY

3.1 Chemicals

The list of chemicals that were used in this study including with their molecular formula and manufacturer are shown in Table 3:1.

Table 3:1 List of chemicals

Chemical	Molecular Formula	Manufacturer
Sodium Silicate, 98%	Na ₂ O ₃ Si	Merck
Sodium Hydroxide, 99%	NaOH	Merck
Pluronic P123, MW: 5800	EO ₂₀ -PO ₇₀ -EO ₂₀	Aldrich
Tetraethylorthosilicate, 98%	TEOS	Merck
Hydrochloric acid, 37%	HCl	Merck
Nickel (II) nitrate hexahydrate, 99%	Ni(NO ₃) ₂ ·6H ₂ O	Merck
Hexadecyltrimethylammonium bromide, 99%	C ₁₉ H ₄₂ BrN	Aldrich
Hydrogen cylindrical tank, >99.99%	H ₂	-
Carbon dioxide cylindrical tank, >99.99%	CO ₂	-
Methane cylindrical tank, >99.99%	CH ₄	-
Nitrogen cylindrical tank, >99.99%	N ₂	-

3.2 Preparation of POFA sodium silica solution

The POFA was obtained from a local palm oil mill located in Pahang, Malaysia. The POFA was calcined at 600°C for 6 h to eliminate excess unburnt biomass debris. The pretreatment of POFA was done with concentrated HCl at 100°C for 3 h under stirring in order to leach out acid-soluble elements. The mixture was then being filtered and the solid residue, denoted as acid-leached POFA (APOFA) was dried 12 h at 110°C before calcined at 600°C for 6 h. X-ray Fluorescence Spectrophotometry (XRF, Bruker S8 TIGER ECO) analysis of POFA and APOFA were performed to verify the composition of the POFA and APOFA. According to XRF analysis, SiO₂ is the major constituent of

POFA (47.62%) and APOFA (67.76%) which indicates that POFA is an alternative low-cost material for commercial sodium silicate (Na_2SiO_3) and pretreatment of POFA with HCl is required to improve the purity of SiO_2 in POFA.

Silica was extracted from APOFA by using alkali fusion treatment adapted from method of Chandrasekar et al., (2008). In brief, APOFA with particle size less than 200 μm was mixed with sodium hydroxide powder (NaOH, Merck) and fused in a furnace for 1 h. The NaOH fused POFA was cooled to room temperature and grounded to fine particle size of 100 μm . Thereafter, the fine particle of the fused POFA was mixed with water, H_2O and stirred at room temperature for 24 h. The resulting suspension was filtered to separate the suspended particles, and supernatant called POFA sodium silicate (Na_2SiO_3 -POFA) was produced. Several extraction process parameters were studied to find the optimal silica concentration of POFA sodium silicate (Na_2SiO_3 -POFA) including mass ratio of NaOH/POFA (0.5:1-4:1), alkaline fusion temperature (400-700°C) and mass ratio of H_2O /NaOH-fused POFA (2:1-6:1). The optimal silica concentration was used for the synthesis of mesoporous SBA-15.

3.3 Synthesis of SBA-15 support

The SBA-15 was synthesized in accordance with the in-depth procedures discovered by Zhao and co-researchers (Zhao et al., 2016). In brief, dissolution of the triblock copolymer $\text{EO}_{20}\text{PO}_{70}\text{EO}_{20}$ (P123, Aldrich) was done at 40°C in concentrated hydrochloric acid (HCl, Merck) solution under vigorous stirring for 1 h. The Na_2SiO_3 -POFA was then added dropwise into the mixture under constant agitation for 24 h at 40°C, and the white sediment was acquired. The sediment was rinsed with deionized water, filtered and also air-dried for 12 h at 110°C before being calcined at 550°C using muffle furnace for 3 h to eliminate the template. SBA-15 (R2.0), (R2.9) and (R4.0) were prepared with distinct mass ratios of Na_2SiO_3 -POFA/P123 (2.0, 2.9 and 4.0). According to the previous study reported by Fazaeli et al., (2012) for commercial sodium silicate (Na_2SiO_3), the optimum Na_2SiO_3 /P123 mass ratio for SBA-15 preparation was found to be at 2.9. Therefore, mass ratios of Na_2SiO_3 -POFA/P123 (2.0, 2.9 and 4.0) were proposed for easier comparison with commercial SBA-15 and to avoid controversial comparison. Additionally, commercial SBA-15 was synthesized using commercial sodium silicate (Na_2SiO_3 , Merck) in which sodium silicate/P123 ratio = 2.9 by following the similar procedures, and the sample was designated as SBA-15(Comm.).

3.4 Preparation of Ni/SBA-15

Typical incipient wetness impregnation technique was adopted over Ni/SBA-15 preparation whereby SBA-15 was subjected into a dissolved solution of 5wt% Ni salt precursor, $\text{Ni}(\text{NO}_3)_2 \cdot 6\text{H}_2\text{O}$ (Merck, 99%). The obtained slurry was then heated under continuous stirring at 80°C to evaporate the major water content. Calcination of the solid remnants was done at 550°C for 3 h after being dried for 12 h at 110°C .

3.5 Catalyst characterization

The crystalline texture of the catalysts was examined via X-ray diffraction (XRD) recorded over powder diffractometer (Philips X' Pert MPD, 30 kV, 15 mA) within the range of $2\theta = 10^\circ - 80^\circ$ with a $\text{Cu K}\alpha$ radiation ($\lambda = 1.5405\text{\AA}$). The average NiO crystal size was determined by using Scherrer equation.

The specific surface areas, average pore diameters and total pore volume of the catalysts were examined under -196°C liquid nitrogen using AS1 MP-LP analyzer of AUTOSORB-1 model. The samples were evacuated under N_2 atmosphere for 3 h at 300°C before chemisorption process. The specific surface areas were obtained using Brunauer-Emmett-Teller (BET) equation, whereas porosity of the catalysts was confirmed using Barrett-Joyner-Halenda (BJH) method.

To identify the functional group of the catalysts and the Ni species interaction with SBA-15, KBr pellet through Thermo Nicolet Avatar 370 DTGS model was used to perform Fourier Transform Infrared (FTIR) testing. Under the operation of 80 kV, the catalyst's morphology was viewed via a (ZEISS SEM EVO-50 model Scanning Electron Microscope. With an accelerating voltage of 300 kV, transmission electron micrographs (TEMs) observations were executed on a JEM-2100 Electron Microscope. Prior to the viewing, the samples were scattered homogeneously in ethanol and being dropped onto a porous, amorphous carbon grid before being subjected to drying.

In the current study, characterization of basic sites was done using pyrrole as a probe molecule due to its weak acidity and ability to be adsorbed reversibly. FTIR measurements of this analysis were conducted on a high-temperature stainless steel cell CaF_2 windows equipped Agilent Cary 640 FTIR spectrometer in transmission mode. At 400°C , 0.03 g of self-supported wafer form sample was degassed in 100 mL/min H_2 flow

for 2 h and cooled to ambient temperature under He atmosphere. Then, 2 Torr of pyrrole was exposed to the reduced catalyst at room temperature for 0.5 h, accompanied with degassing for 5 min at five different temperatures of 30°C, 50°C, 100°C, 150°C and 200°C, respectively. By using the 5 cm⁻¹ spectral resolution, all spectra were recorded at ambient temperature.

3.6 CO₂ reforming of CH₄

The catalytic activity of CO₂ reforming of CH₄ was conducted under ambient pressure in stainless steel packed bed reactor (i.d. 11 mm, length 417 mm) (Figure 3:1) under gas hourly space velocity (GHSV) of 15,000 mLg⁻¹h⁻¹ within 24 h time-on-stream (TOS). 0.2 g of catalyst was loaded on a quartz wool plug in the tubular reactor. The reaction temperature was precisely measured by a temperature-controlled furnace. Before the reaction started, the catalyst was reduced in 50 mL/min of H₂ flow at 700°C for 1 h. The reaction took place at 800°C with 50 mL/min of total volumetric flow rate (CH₄ and CO₂), with a ratio of CH₄:CO₂ = 1:1. N₂ played a role as the carrier gas with a flow rate of 25 mL/min. The effluent and reactant gas components were analyzed by a thermal conductivity detector (TCD) type of agilent gas chromatography (AGILENT 6890 N). The conversion of CH₄ and CO₂, the ratio of H₂/CO are determined as follows:

$$\text{CO}_2 \text{ Conversion, } X_{\text{CO}_2} = \frac{F_{\text{CO}_2,\text{in}} - F_{\text{CO}_2,\text{out}}}{F_{\text{CO}_2,\text{in}}} \times 100 \quad 3.1$$

$$\text{CH}_4 \text{ Conversion, } X_{\text{CH}_4} = \frac{F_{\text{CH}_4,\text{in}} - F_{\text{CH}_4,\text{out}}}{F_{\text{CH}_4,\text{in}}} \times 100 \quad 3.2$$

$$\frac{\text{H}_2}{\text{CO}} = \frac{F_{\text{H}_2}}{F_{\text{CO}}} \quad 3.3$$

Where F represents the molar flow rate for a particular component in mL/min.

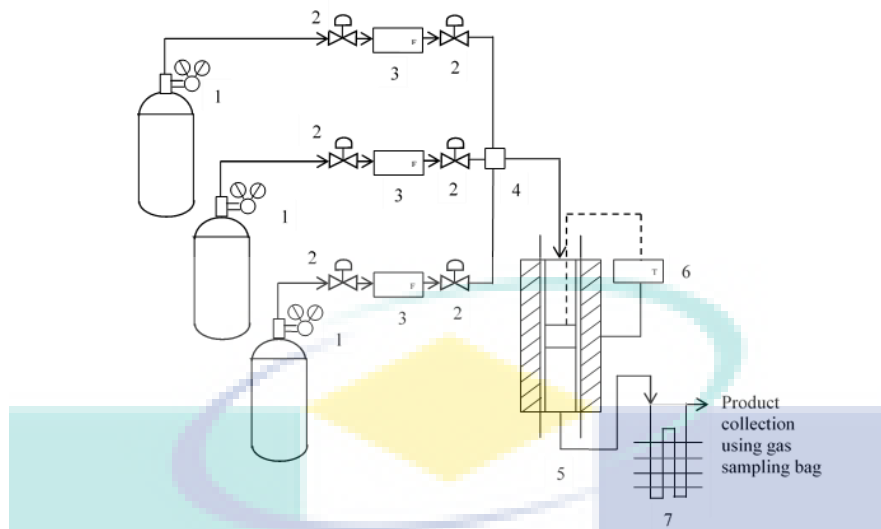


Figure 3:1 Process flow diagram of the CO₂ reforming of CH₄. (1) Regulator, (2) valve, (3) mass flow controller, (4) gas chamber, (5) vertical tube furnace, (6) temperature controller, (7) condenser

UMP

CHAPTER 4

RESULTS AND DISCUSSION

4.1 Effect of extraction parameter on concentration of extracted silica

In order to achieved the optimum silica content, various extraction parameters were studied including mass ratio of NaOH/POFA (0.5:1-4:1), alkaline fusion temperature (400-700°C) and mass ratio of H₂O/NaOH-fused POFA (2:1-6:1).

4.1.1 Effect of mass ratio of NaOH/POFA

The effects of NaOH/POFA mass ratio in the range of 0.5 – 4 were studied. The Si concentration of extracted solutions, which were prepared from different mass ratios of NaOH/POFA are shown in Figure 4:1. As can be seen in Figure 4:1, the highest Si content was obtained from the extracted solution at NaOH/POFA mass ratio of 2 which is 40570 ppm, followed by NaOH/POFA mass ratio of 1, 4 and 0.5 with value of Si contents are 36130 ppm, 32330 ppm and 27720 ppm, respectively. This result shows that alkali reacts with amorphous silica in POFA at a 2:1 mass ratio producing high sodium silicate due to the optimum process of Si-O-Si hydrolysis. The different in silica content obtained at different mass ratio might related to the changes in the pH of solution, and thus changing the dissolution process of silica in aqueous solution (Manuscript & Processes, 2013). According to Sousa et al. (Macromoleculas et al., 2009), the configuration of Si-O-Si bonds has strong influence on the extraction process of silica that will affect the final amount of extracted silica. This mass ratio of NaOH/POFA was taken to be the optimum and was kept constant in the subsequent experiment.

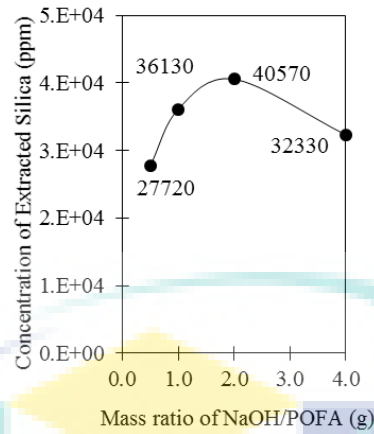


Figure 4:1 Effect of NaOH/POFA mass ratio on concentration of extracted silica

4.1.2 Effect of fusion temperature

The effects of fusion temperature in the range 400 – 700°C on the concentration of extracted silica from POFA are shown in Figure 4:2. It can be seen that the concentration of extraction silica increased with an increase in reaction temperature up to 550 °C. Yılmaz and Pişkin (2013) reported the similar optimum fusion temperature for the extraction of silicon from tailings slurry of gold mine treatment plant by alkali fusion technique. They found that the fusion of NaOH with slurry most suitable at temperature 550oC. However higher fusion temperature than 550oC will lead to the degradation of chemical compounds and consequently decrease the silica extraction efficiency.

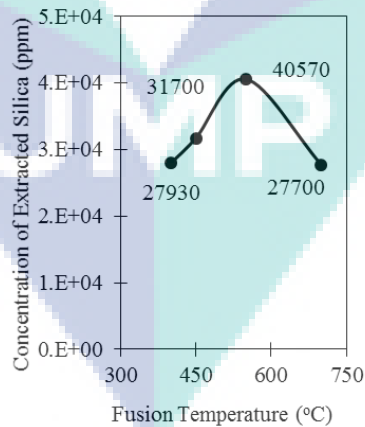


Figure 4:2 Effect of fusion temperature on concentration of extracted silica.

4.1.3 Effect of mass ratio of H₂O/NaOH-fused POFA

The effects of mass ratio of H₂O/NaOH-fused POFA on extraction of silica for 2, 3, 4 and 6 are shown in Figure 4:3. Based on the result obtained, the use of small amounts of H₂O decreased the leaching process of sodium silicate due to the higher viscosity of the solution that led to the harder solid–liquid separation process. The highest silica content was achieved at mass ratio of H₂O/NaOH-fused POFA of 4:1. This result might due to the suitable viscosity of the solution that contributing to enhance the extraction process effectively. This trend is agreements with the previous research done by Silva et al. (2012) that study the effect of H₂O/NaOH-fused Brazillian zircon on extraction of zircon.

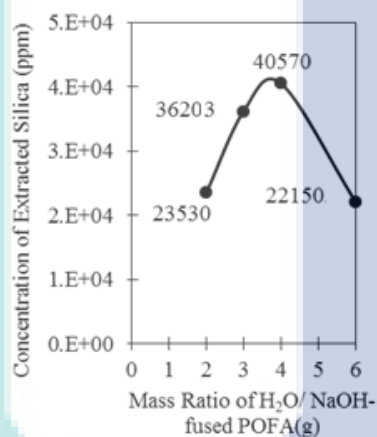


Figure 4:3 Effect of H₂O/NaOH-fused POFA mass ratio on concentration of extracted silica.

4.1.4 Outcomes of the study

The preparation of POFA sodium silicate (POFA-Na₂SiO₃) was done using sodium hydroxide (NaOH) fusion method under several parameters including NaOH/POFA mass ratio, fusion temperature and H₂O/NaOH-fused POFA mass ratio. The optimum concentration of extracted silica with value of 40570 ppm was obtained at NaOH/POFA mass ratio, fusion temperature and H₂O/fused POFA mass ratio at 2, 550°C and 4, respectively.

4.2 Effect of Na₂SiO₃-POFA/P123 mass ratios on the properties and catalytic activity of Ni/SBA-15 towards CO₂ reforming of CH₄

The modifications of Ni/SBA-15 with distinct Na₂SiO₃-POFA/P123 mass ratios were prepared to identify the optimum ratio for Ni/SBA-15 synthesis. Furthermore, the

influence of silica/surfactant ratio towards properties and catalytic activity of Ni/SBA-15 were evaluated.

4.2.1 Characterization of the catalyst

An exhaustive SBA-15 phase composition analysis was conducted using wide-angle XRD in the range of $2\theta = 10^\circ - 80^\circ$ as illustrated in Figure 4:4. At $2\theta = 15-35^\circ$, the broad hump diffraction peaks expressed the SiO_2 framework of SBA-15 support's reflection peak (Li et al., 2015). It is obvious that all four patterns displayed one broad hump at $2\theta = 22^\circ$, which postulated that the obtained Ni/SBA-15 samples are apparently amorphous (Chiker et al., 2003). Furthermore, the XRD pattern of Ni/SBA-15 catalysts displayed diffraction peaks of NiO at 37.33° , 43.42° , 62.99° and 75.47° , which corresponding to crystalline nickel oxide (NiO) with face-centered cubic structure (Kaydouh et al., 2016). The peaks intensities of NiO increased with increasing mass ratios of Na_2SiO_3 -POFA/P123 from 2.0 to 4.0, indicating the influence of Na_2SiO_3 -POFA/P123 ratio on the location of the NiO. It is suggested that at a higher ratio (Na_2SiO_3 -POFA/P123 = 4.0), the majority of the NiO particles were located at the exterior appearance of SBA-15, whereas, at a lower ratio (Na_2SiO_3 -POFA/P123 = 2.0), the NiO nanoparticles were mostly mounted into the pores of SBA-15. The result observed in this study was in concordance with the finding indicated by Bukhari et al. (2017), which found that the silica-to-surfactant mass ratios remarkably influenced the location of the NiO.

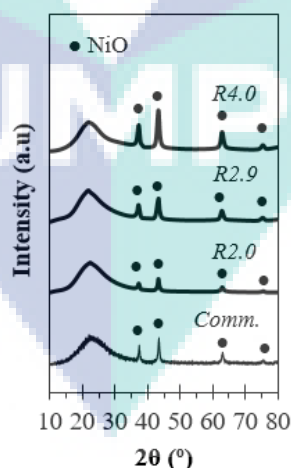


Figure 4:4 XRD pattern of Ni/SBA-15(Comm.) and Ni/SBA-15 with Na_2SiO_3 - POFA/P123 mass ratios of 2.0, 2.9 and 4.0.

Table 4:1 shows the average crystallite dimensions of NiO particles computed using Scherrer equation. Generally, the NiO crystallite sizes of catalysts were 19.12, 14.80 and 23.62 nm for Na₂SiO₃-POFA/P123 mass proportions of 2.0, 2.9 and 4.0 respectively. The largest NiO crystallite dimension at higher silica-to-surfactant ratio (Na₂SiO₃-POFA/P123 = 4.0) was most probably related to the blockage of NiO from entering the pores due to the existence of microporous plugs. This resulted to the NiO agglomeration on the exterior appearance of the SBA-15, in conformity with our previous study on the effect of TEOS/P123 (Bukhari et al., 2017). The increment of the crystallite size at higher silica-to-surfactant ratio was also declared by Fouad et al. (2006) for ZSM-5. They found that the mixture's alkalinity increased with the silica-to-surfactant mole ratio increment, leading to the decrement in the crystallization rate and enhance in the crystallite size of ZSM-5.

Table 4:1 Physical attributes of Ni/SBA-15(Comm.) and Ni/SBA-15 with Na₂SiO₃-POFA/P123 mass ratios of 2.0, 2.9 and 4.0.

Catalyst	Na ₂ SiO ₃ -POFA/P123	BET surface area (m ² /g)	Pore volume (cm ³ /g)	Pore diameter (nm)	d _{NiO} ^a (nm)
Ni/SBA15(Comm.)	-	235	0.44	9.57	15.60
Ni/SBA15(R2.0)	2.0	127	0.38	12.60	19.12
Ni/SBA15(R2.9)	2.9	179	0.33	6.42	14.80
Ni/SBA15(R4.0)	4.0	263	0.26	4.68	23.62

^a Calculated from XRD using Scherer equation.

The textural properties of Ni/SBA-15 in the aspect of the ratio of Na₂SiO₃-POFA/P123 are tabulated in Table 4:1. The BET surface area, pore diameter and pore volume of Ni/SBA-15(Comm.) were 235 m²/g, 0.44 cm³/g, and 9.57 nm, respectively. In correlation with the effect of the Na₂SiO₃-POFA/P123 ratio, it was elucidated that the catalysts' BET surface areas increased in a linear manner with the increment of Na₂SiO₃-POFA ratio. However, the pore diameter and pore volume marked the opposite trend with an increment of the quantity of Na₂SiO₃-POFA. The small pore volume and pore diameter by Ni/SBA-15(R4.0) might be related to the excessive Na₂SiO₃-POFA which led to the enhanced condensation of Si-O-Si formation on the micelles in the catalyst, leading to the disrupted siloxane network structure in the pore walls (Abdullah et al., 2010). Moreover, agglomerated Ni nanoparticles were inadequate to fill superfluous unconfined pores and located at the support's exterior surface, therein resulted in the highest surface area (263 m²/g). On the other hand, the lowest surface area (127 m²/g) indicated by

Ni/SBA-15(R2.0) could be attributed to the deformed silica network on the micelles accompanied by deficiency of Si-O-Si framework conformation condensation, thus affected the pore structure of the sample. This can be claimed to the limited amount of Na_2SiO_3 -POFA to aid in the building of the silica framework for Ni/SBA-15(2.0). Therefore, it is reasonable to claim that Na_2SiO_3 -POFA of 2.9 is the optimal ratio for the synthesis of Ni/SBA-15 from Na_2SiO_3 -POFA. Moreover, Ni/SBA-15(R2.9) has an advantage in term of lower NiO crystallite size than that of Ni/SBA-15(Comm.). It is expected that the finer NiO particle size favoured the catalytic performance as it will result in better Ni nanoparticles distribution over the surface in conformity with the study reflected by Sidik et al., (2016).

The N_2 adsorption/desorption isotherms and pore size distribution of Ni/SBA-15 catalysts were plotted in Figure 4:5(A) and Figure 4:5(B), respectively. The adsorption-desorption isotherm of all catalysts corresponded to a reversible type IV isotherm and compromise H1 type hysteresis loop in the IUPAC classification. In brief, the type IV isotherm refers to the pore condensation together with hysteresis behaviour between the adsorption and the desorption branch of typical mesoporous materials (Fulvio et al., 2005), meanwhile, H1 hysteresis loop indicated all Ni/SBA-15 samples possess uniform pores at typical mesoporous materials (Sing et al., 1985). For Ni/SBA-15(Comm.), it was confirmed that the majority of the pores of this solid was in between the mesopore range as isotherm plateaued at the relative pressure range of 0.50 to 1.00 (Aziz et al., 2014b). Meanwhile, for Ni/SBA-15(R4.0), the type of H1 hysteresis loop was observed in the $P/P_0 = 0.55-0.65$, indicated agglomerated, spherical and uniform size particles dispersed at the mesoporous material, which in conformity with the XRD and BET findings. This feature also indicated a typical feature of capillary condensation among uniform pores (Liu et al., 2009). Moreover, it was found that Ni/SBA-15(R4.0) catalyst had quite narrow and monomodal pore size distribution, indicating uniform pore size with highest pore size distribution at around 3.75 nm which scattered at the range 3 nm to 20 nm. However, Ni/SBA-15(2.0) catalyst showed different result whereby a weak hysteresis loop was detected at $P/P_0 = 0.9$, corresponding to interparticle pores (Aziz et al., 2014a). In addition, Ni/SBA-15(R2.0) displayed a broad pore size distribution graph which scattered at the range 5 nm – 10 nm, indicating lower structural ordering. In a case of Ni/SBA-15(R2.9), it was observed that its adsorption branch of nitrogen isotherms had virtually superimposed entirely on the desorption branch, evidencing reversible pore emptying as

well as pore filling (Aziz et al., 2014a). Besides, it is noticed that there is an absence of interparticle pores at about $P/P_0 = 0.9$ for Ni/SBA-15(2.9) catalyst.

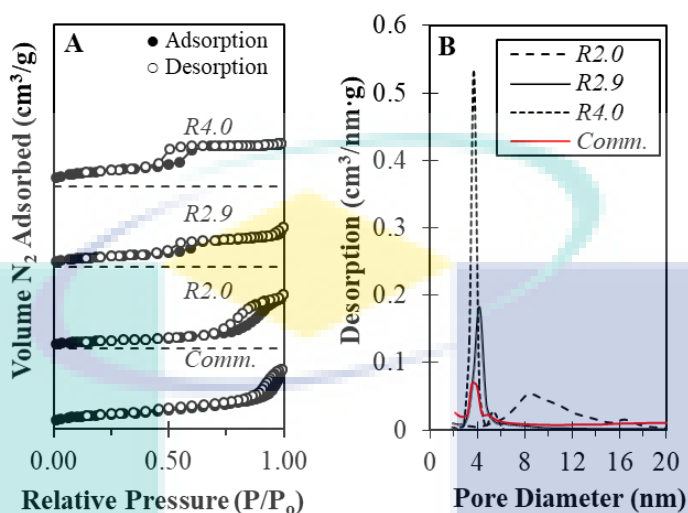


Figure 4:5 (A) N₂ adsorption/desorption isotherms and (B) pore size distribution of Ni/SBA-15(Comm.) and Ni/SBA-15 with Na₂SiO₃-POFA/P123 mass ratios of 2.0, 2.9 and 4.0.

The SEM images of all Ni/SBA-15 catalysts were presented in Figure 4:6. For the effect of Na₂SiO₃-POFA/P123 mass ratios (Figure 4:6(a)-(c)), it is clearly observed that the diversity in Na₂SiO₃-POFA/P123 mass ratios markedly influenced the topology and morphological textures of Ni/SBA-15. Irregular and indefinite morphology of SBA-15 can be seen from the SEM image of Ni/SBA-15(2.0), which could be claimed to the fragmentary condensation phase with insufficient silica source (Na₂SiO₃-POFA). However, the SEM image displayed the comparatively well-defined rod-type structure of SBA-15 with a large amount of clearly defined cavities on its surface for the case of Ni/SBA-15(R2.9). This result might be associated with the optimal ratio of Na₂SiO₃-POFA/P123 which contributed to the favorable hydrolyzation and condensation of the silica precursor in the copolymer micelles. Meanwhile, when the Na₂SiO₃-POFA/P123 mass ratios 4.0 was used, multitudinous pores were formed on the catalyst surface and thus resulted in a distorted irregular shape of SBA-15. It is suggested that the excessive amount of Na₂SiO₃-POFA deterred the appropriate configuration of the Si-O-Si framework by obstructing silica framework from condensing around the micelles. Additionally, the excessive quantity of Na₂SiO₃-POFA was also hydrolysed and condensed in copolymer micelles to form microporous nanocapsules, and thus resulted in distorted irregular shape (Kruk et al., 2003). The impact of silica-to-surfactant ratio on

the morphology and shape of material was also affirmed by (Fouad et al., 2006) for ZSM-5 catalyst. They claimed that the diversity in surfactant-to-silica mole ratios markedly influenced the morphology and shape of ZSM-5 catalyst whereby different shape (cube-like, sphere-like and network-like) of crystals were formed at different surfactant-to-silica ratios (0.322, 0.43 and 0.537).

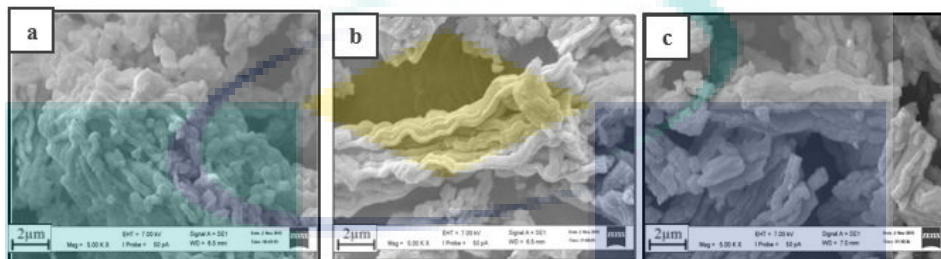


Figure 4:6 SEM micrographs of Ni/SBA-15 with Na_2SiO_3 -POFA/P123 mass ratios of (a) 2.0, (b) 2.9 and (c) 4.0.

The morphological structures and NiO incorporations of the catalysts were determined by TEM, as depicted in Figure 4:7. The existence of NiO nanoparticles in the Ni/SBA-15 catalysts was observed through darker contrast areas of small spots. The Ni/SBA-15(R2.0) showed the entirely distorted array, with the bigger size of NiO. The distortion in a hexagonal array of Ni/SBA-15(R2.0) might postulated the insufficient Na_2SiO_3 -POFA that subsequently caused dissatisfactory silica precursor's condensation phase. Excitingly, the TEM image of Ni/SBA-15(R2.9) showed relatively uniform well-defined, ordered hexagonal arrays of mesopore channels. In addition, the size of NiO at the catalyst's surface is considered small as compared to other ratios. Meanwhile, for Ni/SBA-15(R4.0), it was observed that indistinct hexagonal array present on account of sectional faulty in the Si-O-Si framework formation into a hexagonal matrix with an inappropriate amount of Na_2SiO_3 -POFA and surfactant. Moreover, as shown in TEM image, the majority of the NiO were situated at the exterior appearance of Ni/SBA-15(4.0) with large sizes, representing the NiO agglomerated on the catalyst surface, in line with XRD analysis. The influence of silica-to-surfactant ratios on the topology of SBA-15 was persistent with the research declared by Abdullah et al. (2010) and Miyazawa & Inagaki (2000).

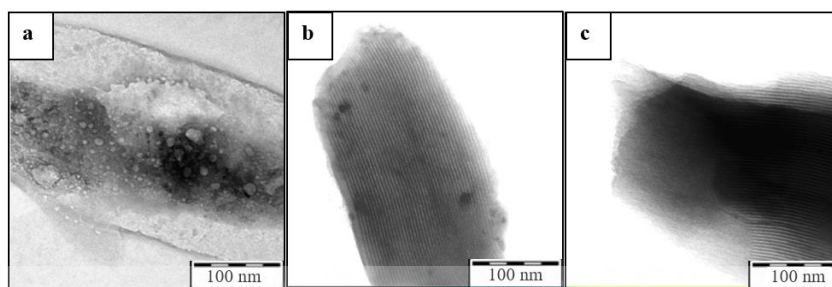


Figure 4:7 TEM micrographs of Ni/SBA-15 with Na_2SiO_3 -POFA/P123 mass ratios of (a) 2.0, (b) 2.9 and (c) 4.0.

The interaction of the atoms and configuration of synthesized Ni/SBA-15 catalysts were studied at a skeletal region between $1400\text{-}500\text{ cm}^{-1}$ of FTIR spectroscopy (Figure 4:8). The absorption bands at roughly 1060 cm^{-1} and 801 cm^{-1} are attributed to asymmetric stretching and symmetric elongation of O–Si–O bending vibration within the framework, respectively (Wang et al., 2014; Ye et al., 2011). In the meantime, the band at 510 cm^{-1} represented the tetrahedrally Si-O-Si bonds bending vibration (Setiabudi et al., 2012). Ni/SBA-15(Comm.) shows well formation of all bands indicating the good ordering of silica framework in Ni/SBA-15(Comm.). It was clearly observed that the mass ratios of Na_2SiO_3 -POFA/P123 did not significantly affect the bands at 801 and 510 cm^{-1} , but markedly influence the intensities of the bands at 1060 and 960 cm^{-1} . It was observed that the intensity of the band at 1060 cm^{-1} was weaker for Ni/SBA-15(R2.0) and Ni/SBA-15(R4.0) in comparison with the Ni/SBA-15(R2.9) demonstrating the imperfection in the Si–O–Si formation at Na_2SiO_3 -POFA/P123 mass ratios of 2.0 and 4.0 due to the inappropriate amount of Na_2SiO_3 -POFA and surfactant. In general, the band approximately 960 cm^{-1} is used to indicate the active metal ions incorporation onto the silica mesopores (Setiabudi et al., 2018) and Si-O-Ni interaction (Ahmed et al., 2012) whereby these interactions were determined by a decline in peak strength and the enveloped peak at the 1060 cm^{-1} band. It was discerned that metal-support interaction within the silica lattice was increasing follow the trend of Ni/SBA-15(R2.0) \approx (R4.0) < (R2.9), suggesting the highest interaction amidst metal-support in Ni/SBA-15(R2.9). The strong interaction amidst active metal and support in Ni/SBA-15 probably due to the perfectly aligned hexagonal conformation of SBA-15(R2.9). Ni/SBA-15(R2.9) was further characterized using IR spectra of adsorbed pyrrole in an attempt to study the basicity characteristics of the catalyst.

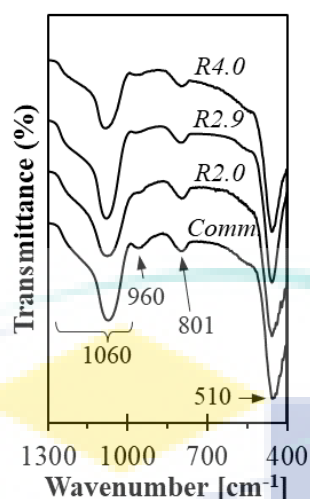


Figure 4:8 FTIR spectra Ni/SBA-15(Comm.) and Ni/SBA-15 with Na_2SiO_3 -POFA/P123 mass ratios of 2.0, 2.9 and 4.0.

The IR spectra of adsorbed pyrrole on Ni/SBA-15(Comm.) and Ni/SBA-15(R2.9) are displayed in Figure 4:9. The wide peak at $3600\text{--}3200\text{ cm}^{-1}$, denoted to the interaction between framework oxygen atoms' basic sites and perturbed N-H stretch of pyrrole molecules, resulting to the formation of $\text{C}_4\text{H}_4\text{NH}\text{--O}$ bridges with basic oxygen (Aziz et al., 2014a). The intensity of the peak decreased with an increased in outgassing temperature, indicating the higher amount of weak basic sites in both catalysts. The peak at 3467 cm^{-1} is accredited to the interaction between the catalyst surface and the perturbed pyrrole molecules' N-H stretch (Sing et al., 1985). Meanwhile, the shoulder peaks observed at 3530 cm^{-1} and 3650 cm^{-1} are attributed to the interaction of N-H stretching of pyrrole with the Si-OH (Aziz et al., 2014a) and bridged hydroxyl groups (Scokart & Rouxhet, 1980). It is clearly indicated that the intensities of the peaks are more intense in Ni/SBA-15(R2.9) than in Ni/SBA-15(Comm.). The less intense peaks in Ni/SBA-15(Comm.) can be linked to the partial Ni blockage which consequently reduce the tendency of pyrrole coverage onto its active sites that are available on the catalyst surface. According to the IR spectra of pyrrole adsorbed, it can be speculated that the basicity of Ni/SBA-15(R2.9) is higher than that of Ni/SBA-15(Comm.). This result most probably attributed to the more available sites for the adsorption of pyrrole in Ni/SBA-15(2.9) resulted from the plentiful silanol groups and the existence of metal-impoverished Ni_2O_3 (Sidik et al., 2016). It is suggested that the Ni_2O_3 is highly distributed on the Ni/SBA-15(R2.9) catalyst since no peak for Ni_2O_3 was found on XRD patterns (Serrano-Lotina et al., 2012).

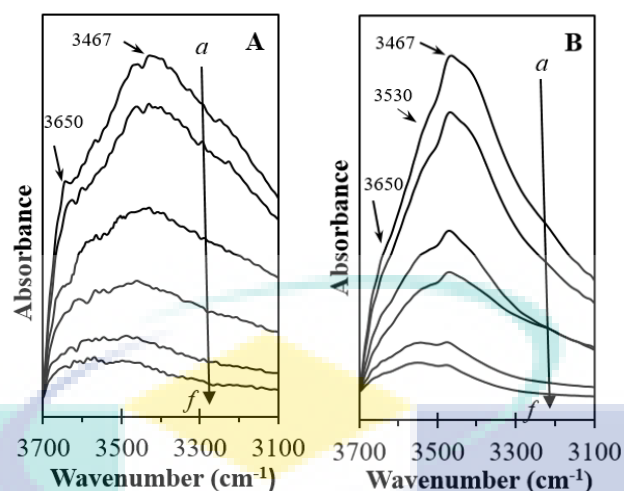


Figure 4:9 IR spectra of pyrrole adsorbed on activated (A) Ni/SBA-15(Comm.) and (B) Ni/SBA-15(R2.9) at (a) room temperature followed by outgassing at (b) room temperature, (c) 50°C, (d) 100°C, (e) 150°C and (f) 200°C.

In general, formation mechanism on the effect of POFA- Na_2SiO_3 /P123 mass ratio over SBA-15 was proposed in Figure 4:10, in which P123 as the template (surfactant) while POFA- Na_2SiO_3 was used as Si-source. P123 are amphiphilic molecule, composed of hydrophilic head and hydrophobic tail. Initially, P123 surfactant molecules favour the arrangement on the water surface and tend to form spherical micelles in water due to their amphiphilicity. Subsequently, self-assembly of the micelles occurred to form surfactant micelle rods, followed by elongation and arrangement of the micelles rods in a hexagonal pattern. Then, POFA- Na_2SiO_3 was added to the aqueous surfactant solution and the hydrolysis and condensation of POFA- Na_2SiO_3 was occurred, thus resulted in the building of silica framework around surfactant micelles. From the comparison of the POFA- Na_2SiO_3 /P123 ratio, it was proposed that the optimal mass ratio of 2.9 manage to build an intact SBA-15 silica framework with its appropriate quantity of Si-source in respect to surfactant. Regrettably, POFA- Na_2SiO_3 /P123 = 2.0 was insufficient to aid the completion of the SBA-15 silica framework, which resulted in defective outlook. Meanwhile, for POFA- Na_2SiO_3 /P123 = 4.0, an excessive Si-source has assembled and accumulated around the hexagonal pattern micelles rod, resulted in a superfluous Si surface. Lastly, the surfactants were eliminated and left only the mesoporous silica after the calcination process.

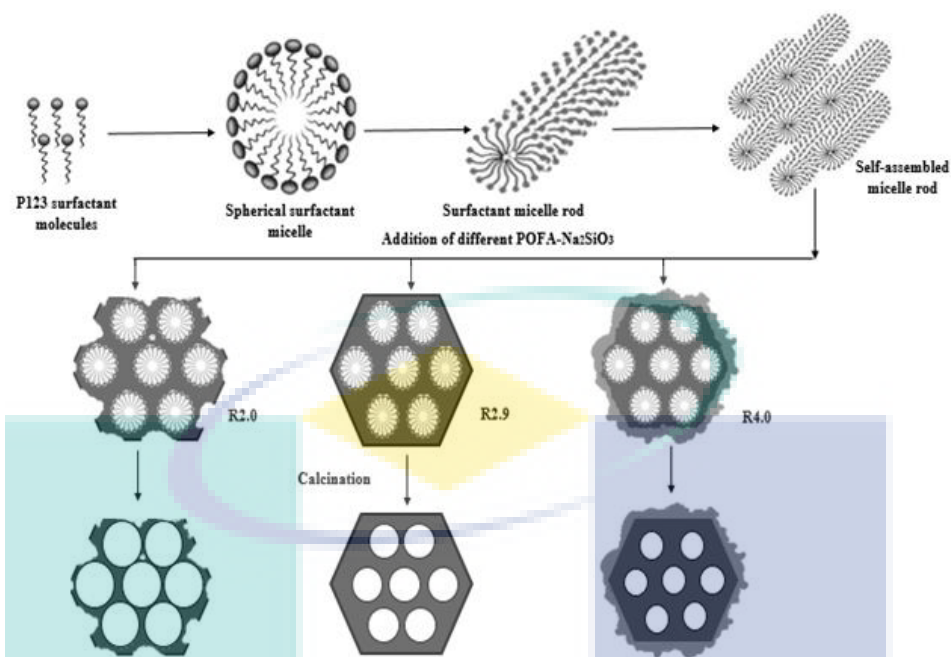


Figure 4:10 Formation mechanism on the effect of POFA- Na_2SiO_3 /P123 mass ratio over SBA-15.

4.2.2 Catalytic performance of the catalyst toward CO_2 reforming of CH_4

The effect of the mass ratio of Na_2SiO_3 -POFA to P123 on the activity of Ni/SBA-15 catalysts over CO_2 reforming of CH_4 were summarized in Figure 4:11(A). It has been found that the CH_4 conversion of all catalysts was greater than that of CO_2 , which might be due to the small extent of methane decomposition as a secondary reaction ($\text{CH}_4 \rightarrow \text{C} + 2\text{H}_2$) (Kaydough et al., 2016). This secondary reaction has promoted some of the CH_4 to be converted into coke and hydrogen in parallel with the primary reforming reaction. The activity of Ni/SBA-15 catalysts decreased with the trend of Ni/SBA-15(Comm.) \approx (R2.9) > (R2.0) > (R4.0), indicating an exceptional catalytic performance of Ni/SBA-15(R2.9) (Conv. CH_4 = 91.4%, Conv. CO_2 = 88.4%) in comparison with Ni/SBA-15(Comm.) (Conv. CH_4 = 92.1%, Conv. CO_2 = 88.9%). The dissimilar in catalytic performance can be ascribed to the number of active metal sites exposed to the reactant molecules. Referring to the suggested mechanism, CO_2 activation mainly occurred at the support whereas the CH_x fragments decomposition accompanied with stepwise adsorption of CH_4 took place on active metal spots for CO_2 reforming of CH_4 (Vafaeian et al., 2013). Thus, the availability of numerous exposed NiO spots for the confinement of the reactant molecules is the key success for the excellent catalytic activity. As observed in characterization results, Ni/SBA-15(R2.9) has ameliorated NiO dispersion

with smaller NiO size (14.8 nm) arose from the strong Ni-support interaction. These favorable structure properties contributed to a greater quantity of vacant active metals sites and thus ameliorated the catalytic activity of Ni/SBA-15. Meanwhile, defective Ni species incorporation, as well as large NiO nanoparticle size, resulted from weak Ni-support interaction led to the lower activity of Ni/SBA-15(R2.0) and (R4.0).

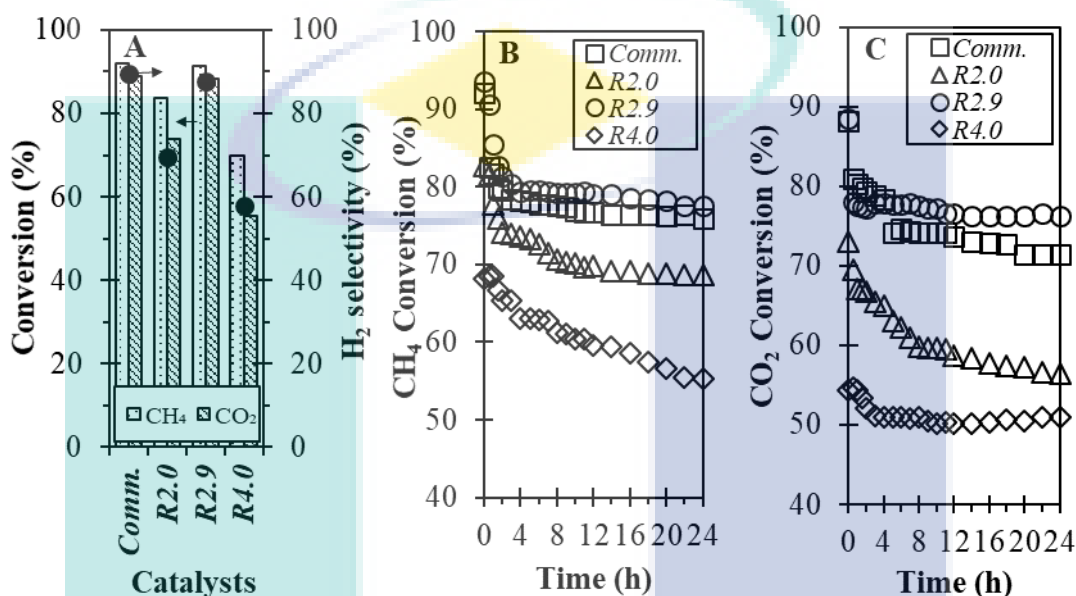


Figure 4:11 (A) Effect of different catalysts on the CH₄ conversion, CO₂ conversion and H₂ selectivity. (B) CH₄ conversion and (C) CO₂ conversion of Ni/SBA-15(Comm.), Ni-SBA-15(R2.0), Ni-SBA-15(R2.9) and Ni-SBA-15(R4.0) towards 24 h time-on-stream (TOS). Reaction conditions: GHSV = 15,000 mLg⁻¹h⁻¹, F = 50 mL/min, CH₄:CO₂=1:1, T = 800°C, P = 1 atm.

In term of H₂ selectivity, Ni/SBA-15(Comm.) showed 89.4%. The H₂ selectivity was in the trend of Ni/SBA-15(R4.0) < (R2.0) < (R2.9), in which the highest H₂ selectivity marked by Ni/SBA-15(R2.9) with 87.6%. This was probably associated with the ideal hexagonal SBA-15 support structure alignment being formed for Ni/SBA-15(R2.9), which offered advanced incorporation of Ni nanoparticles and thereupon led in highest H₂ selectivity. The lowest H₂ selectivity, which is 57.9% for Ni/SBA-15(R4.0) can be claimed to the small extent of the reverse water gas shift reaction (CO₂ + H₂ → CO + H₂O) (Pakhare et al., 2013). This undesired reaction consumed H₂, resulting to the decrement in the H₂ selectivity. In addition, the lowest H₂ selectivity in Ni/SBA-15(R4.0) can also be related to indistinct hexagonal array of Ni/SBA-15(R4.0) on account of the excess amount of Na₂SiO₃-POFA. Meanwhile, the distorted hexagonal array of Ni/SBA-

15(R2.0) due to insufficient Na₂SiO₃-POFA led to the unsatisfactory H₂ selectivity as well (69.5%).

According to the result observed in Figure 4:11(A), it is reasonable to conclude that Ni/SBA-15(R2.9) is the optimal silica-to-surfactant ratio for Ni/SBA-15 synthesized from Na₂SiO₃-POFA, and the influence of Na₂SiO₃-POFA/P123 mass ratios is worth to be explored. It is noteworthy that the synergistic effect of the optimum ratio of SBA-support and availability of exposed NiO sites are the significant factors for determining the efficiency in the CO₂ reforming of CH₄ and high H₂ selectivity.

It is a well-known fact that the CO₂ reforming of CH₄ is always accompanied with side reactions that impede the performance of the catalysts such as methane decomposition ($\text{CH}_4 \rightarrow \text{C} + 2\text{H}_2$) and Boudouard reactions ($2\text{CO} \rightarrow \text{C} + \text{CO}_2$) which are considered as the main contributors to the coke deposition on the catalysts' surface (Haghighi et al., 2007). Formed carbon intermediates tend to grow further to form long-ranged carbon nanotubes in the conditions of high CH₄ conversion. It is acknowledged that the possibility of the coke formation emerged from poor metal support interaction is detrimental to the CO₂ reforming reaction. As illustrated in Figure 4:11(B) and Figure 4:11(C), less prone to coke formation was presumed for Ni/SBA-15(R2.9) compared to the other Na₂SiO₃-POFA/P123 mass ratios, owing to its strongest metal-support interaction as proven in FTIR and its highest stability with the insignificant drop in catalytic stability test. The ability of Ni/SBA-15(R2.9) to inhibit carbon deposition is dependent on the property of CO₂ adsorption and activation (Sidik et al., 2016). Smaller NiO particles size acquired for Ni/SBA-15(R2.9) is beneficial in promoting the carbon nanotubes migration to the catalysts' interface and boosting the carbon intermediates to react with oxygen lattice, thereupon reduced the carbon formation (Li et al., 2015; Zhang et al., 2008). Ni/SBA-15(R2.0) and Ni/SBA-15(R4.0) which encountered the crisis of partial failure in the silica framework formation due to inappropriate Na₂SiO₃-POFA/P123 mass ratios witnessed a lower and less stable catalytic performance, suggesting the deposition of a significant quantity of carbon intermediates. Moreover, Ni/SBA-15(R2.9) showed comparable stability with Ni/SBA-15(Comm.) denoting the satisfactory performance of Ni/SBA-15(R2.9) towards CO₂ reforming of CH₄. By comparing the H₂ selectivity between Ni/SBA-15(R2.9) and Ni/SBA-15(Comm.) (Fig. 8(A)), it was also realized that Ni/SBA-15(R2.9) has comparable H₂ selectivity compared

to Ni/SBA-15(Comm.). This result might be related to high structure defects and basic sites intensity and in the Ni/SBA-15(R2.9) catalyst, as displayed in IR spectra of adsorbed pyrrole (Fig. 6). The existence of defect sites or oxygen vacancies in SBA-15(R2.9) was account for the H₂ formation and thus led to the higher H₂ selectivity of Ni/SBA-15(R2.9) (Özdemir et al., 2010). According to the obtained results, it is reasonable to conclude that POFA has a great potential to be used as the alternative silica precursor of SBA-15 owing to the favorable catalytic properties and efficacy of synthesized Ni/SBA-15. A great potential of waste materials as silica precursor was also reported by Bhagiyalakshmi et al., (2010b) for rice husk ash (RHA). They found that the mesoporous materials (MCM-41, MCM-48, and SBA-15) synthesized RHA has comparable structure properties to those synthesized from conventional silica source. Moreover, the synthesized catalysts have good activities towards the CO₂ adsorption process. In contrast, Pimprom et al., (2015) was successfully synthesized mesoporous silica SBA-15 from RHA with ratios of 0.017SiO₂:0.0003P123:0.1008HCl:2.63H₂O by mole. They found that the ordinary hexagonal structure was obtained by utilizing up to 50% of RHA.

4.2.3 Outcomes of the study

In the present research, a series of Ni/SBA-15 was synthesized using an alternatively low cost and green silica sources, palm oil fuel ash (POFA) and employed in the CO₂ reforming of CH₄. The catalytic performance of Ni/SBA-15 prepared with distinct Na₂SiO₃-POFA/P123 mass ratios has increased with the sequence of Ni/SBA-15(R4.0) < (R2.0) < (R2.9). The characterization results showed that NiO crystallite size is influenced by the metal-support interaction during catalyst preparation, which affected by the Na₂SiO₃-POFA/P123 mass ratios. IR spectra of adsorbed pyrrole verified the presence of high quantity of structure defects sites and high quantity of basic sites in the Ni/SBA-15(R2.9) catalyst, thus increased the number of active sites available for H₂ formation. The Ni/SBA-15(R2.9) catalyst manifested the most excellent catalytic performance as well as the best stability among other ratios, credited to its well-arranged hexagonal mesoporous framework, stronger metal interaction with support, finer NiO nanoparticles size, appropriate average pore size and the higher structure flaws and basicity amount. The remarkable properties of the superior incorporation and fine NiO particles size with the strong basic property and surface defects intensity in the Ni/SBA-

15(R2.9) catalyst confirmed the great potential of POFA as the alternative silica precursor of SBA-15 for hydrogen production.

Since the Ni/SBA-15 with $\text{Na}_2\text{SiO}_3\text{-POFA/P123} = 2.9$ showed highest activity towards CO_2 reforming of CH_4 , $\text{Na}_2\text{SiO}_3\text{-POFA/P123} = 2.9$ was used in the subsequent study.

4.3 Effect of Ni-Loading on the properties and catalytic activity of Ni/SBA-15 towards CO_2 reforming of CH_4

The main attention of this study is to discover the Ni loading (1, 2, 3 and 5 wt%) influence on physicochemical properties of catalyst and catalytic performance of Ni/SBA-15 towards CRM. This was achieved by comparing the reactivity of the Ni/SBA-15 in the CO_4 and CH_4 conversion towards syngas production (H_2 and CO) with their physicochemical properties.

4.3.1 Characterization of the catalyst

Figure 4:12(A) shows the low angle of XRD patterns of parent SBA-15 and 1, 2, 3, and 5 wt% Ni/SBA-15 catalysts. According to works of literature, SBA-15 has a well-defined peak in the range of low angle at 2θ of 0.92° , which indicates the mesostructure of the SBA-15 and indexed as (100) (Aziz et al., 2014a; Chiker et al., 2003; Sing et al., 1985). For parent SBA-15 (Figure 4:12(A)-a), a similar well-resolved peak was also observed, suggesting that the SBA-15 mesostructure was successfully synthesized by the silica sources from waste POFA ($\text{Na}_2\text{SiO}_3\text{-POFA}$). Sahiron et al. (Norsuraya et al., 2016) found the similar peak of XRD when the sugarcane bagasse waste material was used as silica source to synthesize SBA-15. Hence, it was proven that the POFA sodium silicate is comparable with the commercial sodium silicate, and could be used as alternative silica source in synthesizing mesoporous SBA-15. For the Ni/SBA-15 catalysts, the corresponding peak of SBA-15 was also observed for all the Ni/SBA-15 catalysts. This result indicating that the SBA-15 mesoporous structure remained although after the addition of Ni species up to 5wt%. However, the peak was shifted to the higher angle of 2θ as the Ni loading was increased. The changes can be claimed to the contraction of SBA-15 framework due to the high amount of Ni species were incorporated onto the SBA-15. Similar results were observed by Chen et al. (Chen et al., 2009) when copper species were impregnated to the SBA-15 support. The wide-angle XRD patterns of

Ni/SBA-15 catalysts with distinct Ni loading are shown in Figure 4:12(B). The presence of SiO₂ refraction peak of the SBA-15 framework (Miyazawa & Inagaki, 2000) was revealed by an existence of a broad peak at around 23° for all samples. While, the observed five diffraction peaks at 37.30°, 43.23°, 62.94°, 75.52° and 79.35° were assigned as cubic crystalline face-centered nickel oxide (NiO) (Ye et al., 2011). The peaks intensities corresponding to the crystalline phase of NiO were increased as the Ni loading increased. This indicates that more NiO particles were situated on the exterior surfaces of the SBA-15 support as the Ni loading were increased (Setiabudi et al., 2016). This outcome is in correspondence with the XRD trends indicated by Setiabudi et al. (2017). They proved that the crystallinity of SBA-15 was decreased around 14.6 % when the increment of Ni loading up to 10 wt% due to fractional deformation of the SBA-15 structure by Ni particles.

The estimation of NiO crystalline size of Ni/SBA-15 catalyst was calculated via Scherer equation at line diffraction broadening of the NiO (200) at 2θ of 43.2° are tabulated in Table 1. The particle size of NiO increased the trend of 3wt % < 5wt% < 2wt% < 1wt% with 16, 27, 30 and 38 nm, respectively. It was reported that the metal particles size was correlated with the peak intensity of the metal, where highest intensity indicated the larger of metal presence over the catalyst's surface (Taufiq-Yap et al., 2013). Among the catalysts, 5Ni/SBA-15 had the highest NiO peak intensity owing to the larger NiO particle size (27 nm).

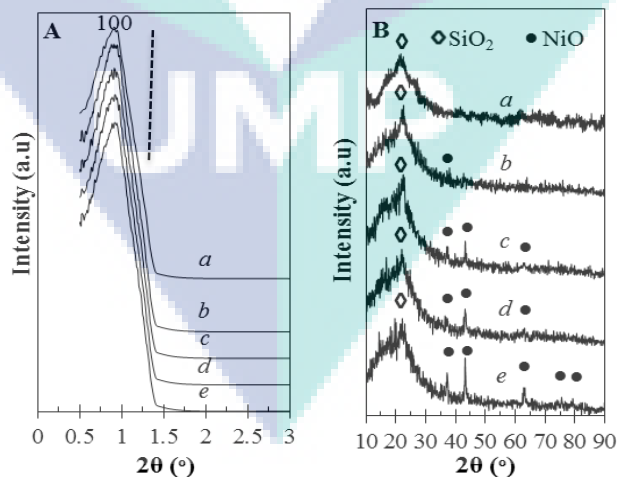


Figure 4:12 (A) Low and (B) Wide angle of XRD patterns of (a) SBA-15, (b) 1Ni/SBA-15, (c) 2Ni/SBA-15, (d) 3Ni/SBA-15 and (e) 5Ni/SBA-15

Table 4:2 Physical properties of SBA-15, 1Ni/SBA-15, 2Ni/SBA-15, 3Ni/SBA-15 and 5Ni/SBA-15.

Catalysts	BET Surface Area (m ² /g)	Pore Volume (cm ³ /g)	Pore diameter (nm)	NiO particle size ^a (nm)
SBA-15	330	0.36	4.52	-
1Ni/SBA-15	326	0.33	5.84	37.96
2Ni/SBA-15	313	0.31	4.50	29.77
3Ni/SBA-15	212	0.25	5.18	16.04
5Ni/SBA-15	190	0.28	5.63	26.74

^aDetermine by XRD (Scherrer equation)

Table 4:2 shows the physicochemical attributes of Ni/SBA-15 catalysts. When POFA sodium silicate was used in the synthesized of SBA-15, 330 m²/g of the BET surface area was achieved. From works of literature, the surface area of the SBA-15 was 699 m²/g and 332 m²/g when the silica sources from TEOS and commercial sodium silicate were used during the SBA-15 synthesis. For comparison, SBA-15 synthesized from TEOS showed the highest surface area, followed by commercial sodium silicate with 332 m²/g (Rahmat et al., 2016) and POFA sodium silicate with 330 m²/g. It is noted that the BET surface area of SBA-15 synthesized from POFA sodium silicate was comparable with the commercial sodium silicate, might be due to the similar chemical structure of both silica sources. Likewise, the huge difference with TEOS silica origins might owing to high silica purity and different chemical structure of TEOS.

As the Ni loading was increased from 1 to 5wt%, the BET surface area and pore volume of Ni/SBA-15 catalysts were decreased from 330-190 m²/g and 0.34-0.25 cm³/g, respectively. This result could be due to the collapsed of other parts within the structure of the SBA-15 and also SBA-15 pore blockage by NiO particles with the increment in Ni loading. The change in BET surface area caused by the introduction of the different amount of metal species is observed in Co/Al₂O₃, reported by Ozkara et al. (2005). They found that BET surface area of 36 wt% Co is smaller than 16.8 wt% Co with the value 214 m²/g and 243 m²/g, respectively. They claimed that it was caused by the blockage of the Al₂O₃ pores with Co particles when introducing higher wt% of Co. The same trends reported by Du et al. when SBA-15 was introduced to the vanadium (Du et al., 2008). They discovered the decline of the BET surface area and pore diameter of V/SBA-15 have occurred when the vanadium percentage on the SBA-15 was increased due to blockage of SBA-15 pores by vanadium species. In addition, the slight increase in the

pore volume of 5Ni/SBA-15 could be related to the expansion of the SBA-15 pores by larger NiO particle size as evidenced by XRD studies. Slight increase of pore volume when loading of 5.1 wt% of Ni was also observed on ZSM-5 in which the pore volume increase to $2.1 \text{ cm}^3/\text{g}$ due to the expansion of ZSM-5 pores with Ni species (Moradi et al., 2016). Thus, the pore volume of 5Ni/SBA-15 was larger than 3Ni/SBA-15 due to the much expansion of the SBA-15 pores when agglomerate Ni particle was contracted with the SBA-15 wall (Setiabudi et al., 2017).

The nitrogen adsorption-desorption of Ni/SBA-15 catalysts are presented in Figure 4:13. The SBA-15 and Ni loaded SBA-15 exhibited type IV isotherms with a clear hysteresis loop of type-H1 (Sing et al., 1985), corresponding to the regular mesoporous features of the SBA-15 (Chandrasekar et al., 2009). This observation reveals that mesoporous nature SBA-15 synthesized from POFA did not destroy when Ni was introduced on SBA-15. As elucidated in Figure 4:13, the 5Ni/SBA-15 showed the lowest nitrogen adsorbed volume compared to others Ni/SBA-15 catalysts, suggesting on the basis of some porosity loss when the higher Ni incorporation on the SBA-15 surfaces. Moreover, Ni/SBA-15 catalysts showed hysteresis loop was shifted to lower P/P° relative pressure after Ni impregnated in SBA-15, demonstrating a slightly SBA-15 porous structure distortion of when incorporating Ni (He et al., 2015).

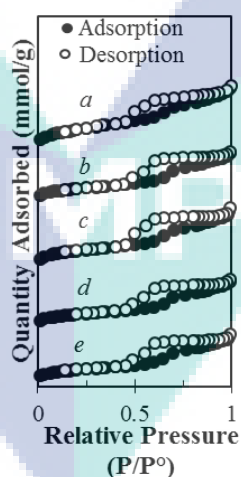


Figure 4:13 Nitrogen adsorption isotherm of (a) SBA-15, (b) 1Ni/SBA-15, (c) 2Ni/SBA-15, (d) 3Ni/SBA-15 and (e) 5Ni/SBA-15.

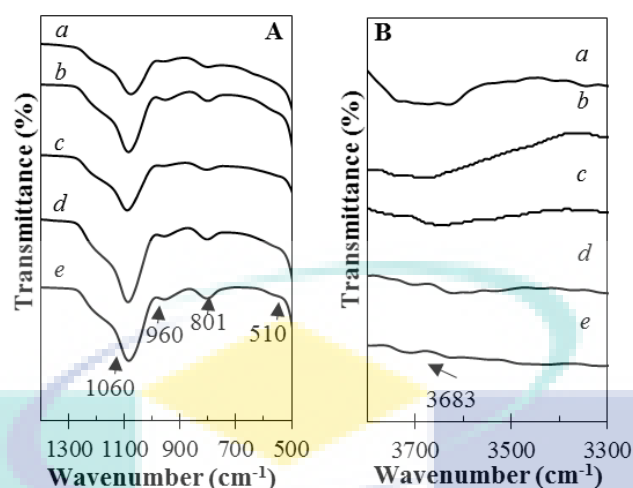


Figure 4:14 FTIR spectra in the range of (A) 1400-500 cm^{-1} and (B) 3800-3300 cm^{-1} of (a) SBA-15, (b) 1Ni/SBA-15, (c) 2Ni/SBA-15, (d) 3Ni/SBA-15 and (e) 5Ni/SBA-15.

Figure 4:14 shows the FTIR patterns of parent SBA-15 and Ni/SBA-15 with distinct Ni loading within the ranges of 3800-3300 cm^{-1} and 1400-500 cm^{-1} . The band detected at 960 cm^{-1} is credited to the Si-OH non-bridging oxygen stretching vibration. A slight decrease of the band is noticed with increasing of Ni loading, which could be related with the substitution of hydrogen atoms in O-H bonds with O-Ni to form Si-O-Ni. The changes in the Si-OH bond at 960 cm^{-1} was also observed in Ni/MSN implied by Sidik et al. (2016). They discovered that the peak intensity at 956 cm^{-1} was decreased due to the -OH group substitution by O-Ni ions possibly happened and creates Si-O-Ni bonding upon Ni addition. The absorption peaks at 1060 cm^{-1} and 801 cm^{-1} were assigned to Si-O-Si asymmetric stretching and symmetric stretching of the SBA-15 framework, respectively. While the absorption peak appears at 510 cm^{-1} was ascribed as the formation of the Si-O-Si bending vibration of SBA-15 framework (Setiabudi et al., 2017). It was notified that the intensities of peaks at 1060, 801 and 510 cm^{-1} did not change by introducing of Ni, indicated no interaction of Ni species with Si-O-Si. In addition, the observed peak at 3683 cm^{-1} in Fig. 3(B), assigning to the Si-OH stretching vibration of O-H in adsorbed H_2O molecules was decreased with the increase of Ni loading. The band changes were due to the replacement of O-H bonds in water molecules with O-Ni when the Ni was introduced. It can be concluded that bands changes at 960 and 3683 cm^{-1} could prove that O-H was substituted by O-Ni for the formation of Si-O-Ni.

Figure 4:15 shows the TEM images of the SBA-15 and Ni/SBA-15 catalysts. Fig. 4(a) demonstrated that the SBA-15 synthesized from POFA has a hexagonal mesoporous

structure like honeycomb-shape. This morphology is similar to the SBA-15 that used commercial silica source during the SBA-15 preparation (Chandrasekar et al., 2008; J. Wang et al., 2013). Therefore, it could be noted that the SBA-15 used in this study was successfully synthesized from waste POFA. For the all Ni/SBA-15, the presence of dark spot appeared in the images were indicated the distribution of Ni dispersion on the SBA-15 support. The distribution of Ni species became very dense with increasing of Ni loading on the SBA-15 support. Some Ni clusters with bigger size around 30-37 nm were visible in the 1Ni/SBA-15 and 2Ni/SBA-15 catalysts. While the formation of smaller Ni particle with well Ni dispersion on the SBA-15 support's surface as observed in the 3Ni/SBA-15 catalyst. The result observed has been verified with the XRD characterization (Figure 4:12) and specific area of the catalyst (Table 4:2).

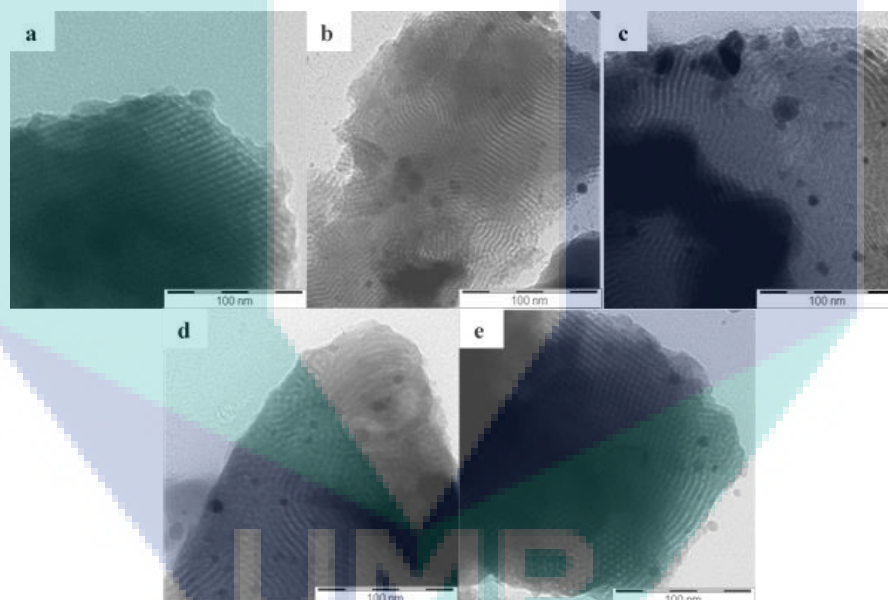


Figure 4:15 TEM images of a) SBA-15, (b) 1Ni/SBA-15, (c) 2Ni/SBA-15, (d) 3Ni/SBA-15 and (e) 5Ni/SBA-15.

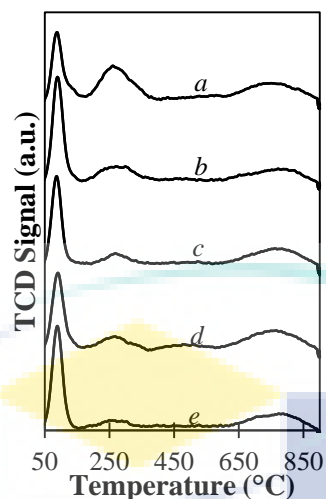


Figure 4:16 CO₂-TPD profile of a) SBA-15, (b) 1Ni/SBA-15, (c) 2Ni/SBA-15, (d) 3Ni/SBA-15 and (e) 5Ni/SBA-15.

CO₂-TPD profile of SBA-15, 1Ni/SBA-15, 2Ni/SBA-15, 3Ni/SBA-15 and 5Ni/SBA-15 catalysts were shown in Figure 4:16. Based on the CO₂-TPD plots, all the catalysts have three types of basic sites in which weak basic sites appear in 100–250°C were attributed to surface hydroxyl group, medium basic sites in 250–550°C were corresponding to medium basic sites, and strong strength of base sites is above 550 °C were linking to adsorption on low undercoordinates O sites (Zhu et al.2012; Zhang et al., 2014) . The amount of desorbed CO₂ was summarized in Table 4:3. The amount of desorbed CO₂ molecules was decreased as increasing of Ni loading on the SBA-15. The results in Table 2 revealed that 1Ni/SBA-15 has the highest total amount of desorbed CO₂ after addition of Ni with 2.5079 mmol/g. While 3Ni/SBA-15 catalyst possesses the highest amount of desorbed CO₂ molecules at the range of strong basic sites with 0.7930 mmol/g. This result indicates that 3Ni/SBA-15 catalyst has the highest capability in adsorbing the acidic CO₂ to its surfaces.

Table 4:3 Amount CO₂-TPD of SBA-15, 1Ni/SBA-15, 2Ni/SBA-15, 3Ni/SBA-15 and 5Ni/SBA-15.

Catalyst	Desorption Peaks	Desorbed CO ₂ (mmol/g)	Total desorbed CO ₂ (mmol/g)
SBA-15	100–250°C	0.8767	2.9196
	250–550°C	1.3310	
	above 550°C	0.7119	
1Ni/SBA-15	100–250°C	1.6039	2.5079

	250–550°C	0.4340	
	above 550°C	0.4700	
2Ni/SBA-15	100–250°C	1.3650	2.3593
	250–550°C	0.2630	
	above 550°C	0.7313	
3Ni/SBA-15	100–250°C	1.1531	2.2150
	250–550°C	0.2690	
	above 550°C	0.7930	
5Ni/SBA-15	100–250°C	1.5530	2.3480
	250–550°C	0.1780	
	above 550°C	0.6170	

4.3.2 Catalytic performance of the catalyst towards CO₂ reforming of CH₄

The influence of 1,2,3,5 wt% of Ni loading on the catalytic performance of Ni/SBA-15 towards CRM was investigated within 24 h time-on-stream (TOS), and the results are given in Figure 4:17(A) and Figure 4:17(B). The average of CH₄ and CO₂ conversions plus H₂/CO ratio are plotted as a function of Ni loading as shown Fig. 6(C), in which more clearly illustrate the effect of different Ni loading on the catalytic activity of Ni/SBA-15 in CRM. The catalytic performance of Ni/SBA-15 catalyst for CO₂ reforming of CH₄ decreased with the order of 3wt% > 5wt% > 2wt% > 1wt% -Ni/SBA-15 meanwhile the H₂/CO ratio followed the order of 3 wt% > 2 wt% > 5 wt% > 1 wt% - Ni/SBA-15. The CO₂ and CH₄ conversions increased in parallel with the increment of Ni amount from 1wt% to 3 wt%, suggesting that more active sites were the presence as loading of Ni increased. More metallic Ni species provided on the surface of catalyst would favor the CRM. However, the CO₂ and CH₄ conversions were reduced when the Ni was loaded up to 5wt% for 5Ni/SBA-15 catalyst. The possible reason is that the agglomeration of Ni species could result in poor Ni species distribution as evidenced by TEM characterization. This behavior could minimize the surface of active sites to contact with CO₂ and CH₄ reactant, and thus leading to loss of active sites to produce syngas. It is notified that the most crucial part in dry reforming of the CH₄ mechanism is CH₄ activation by its decomposition into CH_x fragments that arises on active metal sites of the catalyst, whereby the CO₂ activation mainly take place on the supports surfaces (Huang et al., 2011).

Among the catalysts, highest catalytic performance was achieved over 3Ni/SBA-15 catalyst with the CH₄ and CO₂ conversions were 87.11% and 76.51 %, respectively

and H₂/CO ratio was 0.84. 3Ni/SBA-15 possess high catalytic performance because of the presence of Ni active metal sites that strongly correlates with the interaction amidst Ni and SBA-15. The substitution of Ni species in the SBA-15 framework would increase the connection between the Ni-active sites with the support-SBA-15 (Si-O-Ni) and assist the catalytic CRM. Interaction of metal-support played important roles in achieving excellent performance in CRM was reported by Wang et al. (Wang et al., 2018). They claimed that the strong association of interaction between support and metal will be promoted to the better performance and stability. In addition, the enhancement in the catalytic activity typically related to active sites quantity (Jabbour et al., 2014). The number of Ni species provides by 3Ni/SBA-15 is appropriate because of the larger of SBA-15 surface area in which could result to well-distribution of Ni species active sites. From this, it can strongly be suggested that the excellent performance by 3Ni/SBA-15 can be credited to the high availability of Ni active sites that are accessible for the CH₄ and CO₂ molecules.

The presence of strong basic sites in catalyst on SBA-15 support will improve the catalytic performances. According to Zhang et al. (Zhang et al., 2014), the presence of a strong basic site on Ni/MgO assists in increasing the catalytic activity of CRM. Furthermore, the catalytic performance of the catalyst in CRM is correlated with the presence of strong base on support as mention in the literature (Zhang et al., 2009). The presence of sufficient basic sites in the catalyst is a key factor in determining the catalyst performance as this basicity would affect the tight adsorption of CO₂ to react with other gases. Kathiraser et al. were reported that the conversion of CH₄ has happened from dissociation of CH₄ molecule on the active Ni particles surfaces (Kathiraser et al., 2015). While the conversion of CO₂ has occurred on support surfaces with two continuous steps (Alper & Yuksel Orhan, 2017). The first step is the conversion of CO₂ adsorbed molecules on Ni species, then followed by the CO₂ adsorbed molecules dissociation on O²⁻ basic sites of the basic support. Highest strong basicity possessed by 3Ni/SBA-15, result from CO₂-TPD analysis led to excellent reactant conversion and product yield. This was due to the existence of the highest concentration of surface O²⁻ basic sites in 3Ni/SBA-15 catalyst that accelerate the process of CO₂ molecules adsorption and activation. In addition, the increase of the Ni loading will enhance the basicity of the catalyst itself by increasing the amount of CO₂ molecules desorbed. The enhancement of base sites of the catalyst improved the acidic CO₂ molecules adsorption. According to

Liu et al. (Liu et al., 2018), high amount of basic sites may resist the tighten of CO₂ adsorption at catalyst surfaces and thus would restrict the reaction between CO₂ and CH₄. Thus, this result was correlated with the Liu et al. claim in which 1Ni/SBA-15 have the highest basicity but lowest catalytic performances.

In theory, with the ideal reaction process of CRM ($\text{CH}_4 + \text{CO}_2 \rightarrow 2\text{H}_2 + \text{O}$), the ratio of H₂/CO should be at 1. However, the H₂/CO ratio for all Ni/SBA-15 was less than 1 as shown in Figure 4:17(C). This circumstance might recognize the coexistence of reverse water gas shift reaction (RWGS), $\text{H}_2 + \text{CO}_2 \rightarrow \text{H}_2\text{O} + \text{CO}$ as the side reaction. In brief, the production of H₂ would affect the phenomenon of RWGS reaction, in which the strong competition between RWGS reaction (side reaction) with the dry reforming reaction (main reaction) led to increasing of CO₂ conversion and lowering the H₂/CO ratio (Han et al., 2015). The H₂/CO ratio for all Ni/SBA-15 followed the order of 3Ni/SBA-15 > 2Ni/SBA-15 > 5Ni/SBA-15 > 1Ni/SBA-15. 1Ni/SBA-15 has the lowest ratio of H₂/CO and selectivity toward H₂. This was due to H₂O formation via RWGS reaction as the RWGS is favor on metal particles that its reaction accelerates the sintering process which leads to catalyst deactivation (Taherian et al., 2017). The highest production of H₂O might speed up the sintering process of Ni species present in the catalyst and lead to its deactivation during the reaction process. The highest H₂/CO ratio was achieved by 3Ni/SBA-15 catalyst suggested due to its properties that effectively suppress the RWGS reaction and favor the formation of H₂. In addition, the H₂/CO ratio over 3Ni/SBA-15 is near to unity due to the strong basicity of the catalyst which required to accelerate the DRM process as proved by the CO₂-TPD result.

The 24 h catalytic stability experiments of the Ni/SBA-15 catalysts were conducted at 800 °C. As demonstrated in Figure 4:17 (A) and (B), the stability of Ni/SBA-15 catalyst for CRM followed the order of 3Ni/SBA-15 > 5Ni/SBA-15 > 2Ni/SBA-15 > 1Ni/SBA-15. An obvious deactivation was shown by 1Ni/SBA-15, where the CH₄ conversions and CO₂ conversion were dropped around 55% and 46%, respectively along a 24 h of reaction run. While 3Ni/SBA-15 has a steady catalytic performance up to 24 h with CH₄ and CO₂ conversions are 84% and 80%. The various trend in the catalytic stability of Ni/SBA-15 is most probably because of the different properties of the Ni incorporated with the SBA-15. The existing of good distribution of small Ni particle in 3Ni/SBA-15 catalyst could effectively suppress the carbon formation as proven by TEM

and XRD analysis. While larger Ni particle size was deposited in the 1Ni/SBA-15 exhibited fast deactivation. Li and Zhang (2013) (Li & Zhang, 2013) reported the smaller size of Ni/YS(0.04) showing good stability and lower carbon deposition because of well distributed of metal on its support inhibited its carbon accumulation during the reaction. Moreover, the presence of small Ni particle led to creating a strong metal-support interaction in which this could suppress the coke deposition as referred to Wang et al. (Zhang et al., 2008) report. They claimed that stronger Ni/TiO₂-SiO₂ interaction plays a significant role in preventing the sintering and coking of metal active sites during CRM.

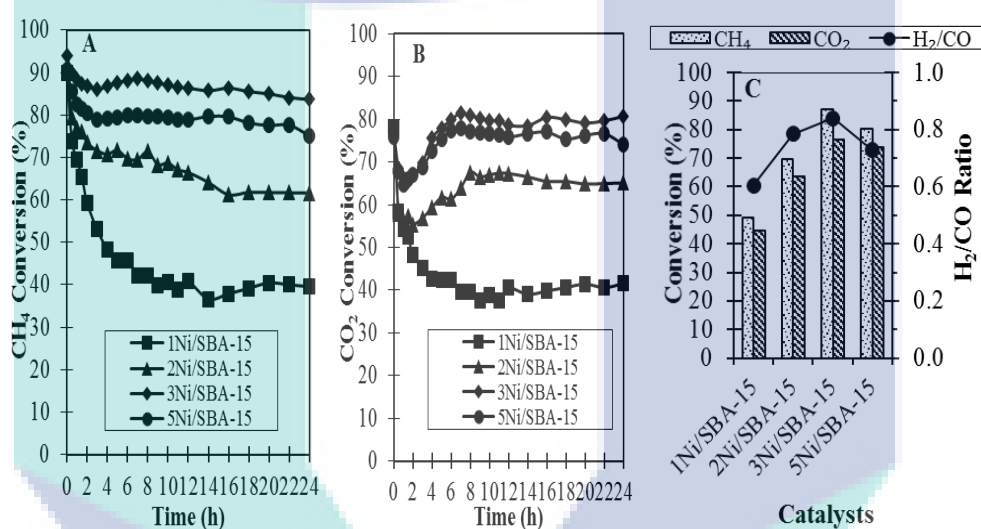


Figure 4:17 (A) CH₄ conversion and (B) CO₂ conversion of Ni/SBA-15 catalysts in CO₂ reforming of CH₄. (C) Effect of different nickel loading on the CH₄ conversion, CO₂ conversion, and H₂/CO ratio. (Reaction conditions: 800°C, CH₄:CO₂:N₂=1:1:1)

4.3.3 Deactivation of catalyst

The XRD patterns of the spent Ni/SBA-15 catalysts were shown in Figure 4:18. It revealed that the diffraction peaks detected at the 2θ values of 26.6° were assigned as graphitic carbon formation. The presence of metallic phase of Ni was observed in the diffraction peaks at 2θ values of 44.5° and 54.7°. It is formed due to the NiO reduction during the reaction. The graphite peaks intensity decrease with the sequences: 1Ni/SBA-15>2Ni/SBA-15>3Ni/SBA-15>5Ni/SBA-15. The graphite carbon was more pronounced for 1Ni/SBA-15 due to the larger of Ni particle size presence on the support surfaces. While small Ni particle size of 3Ni/SBA-15 observed to inhibit less carbon formation. It

was noticeable that large Ni particle catalyst was relatively less active and unstable compared to small Ni particle catalyst towards CRM (Gao et al., 2009). The smaller size of Ni for 3Ni/SBA-15 has helped in reducing the tendency to coke formation process. As in agreement with the literature, a smaller particle size of Ni has been reported to provide positive resistant on the coke formation than the larger size of Ni (Tomishige et al., 1999; Baudouin et al., 2013). In addition, the strong basic sites of 3Ni/SBA-15 supplies more surface oxygen which could prevent the carbon deposition on the catalyst surfaces. Tomishige et al. (Tomishige et al., 1999) stated that more deposition of carbon will be formed on large Ni particle than small Ni particle. Additionally, Wang et al. (Wang et al., 2013) concluded that the metal dispersion of the support surfaces was correlated with the suppression of carbon deposition. The poor Ni dispersion of the 5Ni/SBA-15 catalyst due to the metal agglomeration possibly reduce the metal-surface to have interacted with the reactant. This explanation could be proven by the less intensity of graphite peak of 5Ni/SBA-15 than 3Ni/SBA-15. Thus it can be concluded that the well distribution of small Ni particle on the SBA-15 support could inhibit the carbon deposition rate and useful for the catalytic activity and stability. A similar conclusion was made by the previous study (Chen et al., 2001; Kim et al., 2000).

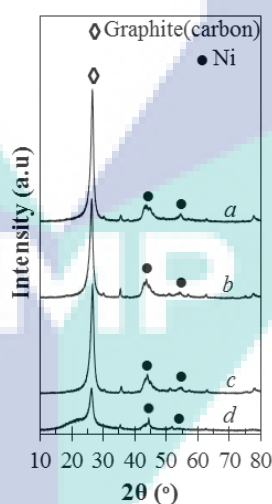


Figure 4:18 XRD pattern of spent catalyst (a) 1Ni/SBA-15, (b) 2Ni/SBA-15, (c) 3Ni/SBA-15 and (d) 5Ni/SBA-15.

4.3.4 Outcomes of the study

Different Ni loadings (1-5 wt. %) of Ni/SBA-15 catalysts, significantly affect the natures and catalytic activities as well as the stability of the catalyst for CRM. The FTIR analysis showed that the metal-support interaction, Si-O-Ni through the substitution of O-H with O-Ni followed the order of 3 Ni/SBA-15 > 5 Ni/SBA-15 > 2Ni/SBA-15 > 1 Ni/SBA-15. The activity and the stability of Ni/SBA-15 catalyst following the trend of 3Ni/SBA-15 (CH₄ conversion = 87.11%, CO₂ conversion = 76.51%, H₂/CO = 0.84) > 5Ni/SBA-15 (CH₄ conversion = 80.11%, CO₂ conversion = 73.91%, H₂/CO = 0.73) > 2Ni/SBA-15 (CH₄ conversion = 69.76%, CO₂ conversion = 63.64%, H₂/CO = 0.78) > 1 Ni/SBA-15 (CH₄ conversion = 49.02%, CO₂ conversion = 44.80%, H₂/CO = 0.60). The outstanding catalytic activity of the 3Ni/SBA-15 in hydrogen production was due to the good incorporation of active Ni species with fine particle size on support and strong Ni and SBA-15 support (Ni-O-Si) interaction. These good properties of 3Ni/SBA-15 could lessen the formation of carbon and help the catalyst to maintain its excellent catalytic activity during the catalytic reaction. The high concentration of surface O²⁻ basic sites in 3Ni/SBA-15 provides more oxygen surface vacancies that helps to minimize the carbon formation during the reaction. While lower catalytic activity over 1Ni/SBA-15 was mostly due to the excess of graphitic carbon accumulated on the SBA-15 surfaces during the reaction run.

The logo of UMP (Universitas Muhammadiyah Purwokerto) is a large, stylized letter 'U' composed of four overlapping triangles in shades of blue and teal. The letters 'UMP' are written in white, bold, sans-serif font across the center of the 'U'.

CHAPTER 5

CONCLUSION

5.1 Conclusion

In this study, Ni/SBA-15 was synthesized using Palm Oil Fuel Ash (POFA) as the silica source and was applied in the CO₂ reforming of CH₄ (CRM). The preparation of POFA sodium silicate (POFA-Na₂SiO₃) was done using sodium hydroxide (NaOH) fusion method under several parameters including NaOH/POFA mass ratio, fusion temperature and H₂O/ NaOH-fused POFA mass ratio. The optimum condition was achieved at NaOH/POFA mass ratio of 2:1, fusion temperature of 550°C and H₂O/NaOH-fused POFA mass ratio of 4:1, with maximum silica content of 40570 ppm.

The obtained POFA-Na₂SiO₃ was used as the silica source for the synthesis of Ni/SBA-15(POFA). A series of Ni/SBA-15(POFA) were synthesized by employing different Na₂SiO₃-POFA/P123 mass ratios (2.0, 2.9 and 4.0) and were compared with Ni/SBA-15 prepared from commercial Na₂SiO₃ (Ni/SBA-15(Comm.)). Na₂SiO₃-POFA/P123 = 2.9 was found to be the optimal synthesis ratio, which produces a well-defined hexagonal framework, smaller NiO particles, stronger Ni-support interaction, homogeneous metal distribution and higher amount of basic sites. The catalytic performance complied with the trend of Ni/SBA-15(R4.0) < Ni/SBA-15(R2.0) < Ni/SBA-15(R2.9) ≈ Ni/SBA-15(Comm.), indicating the excellent catalytic activity of Ni/SBA-15(R2.9). The favorable physicochemical properties of Ni/SBA-15(R2.9) ameliorated the active Ni metals stabilization over SBA-15 and boosted the catalyst's virtues towards an outstanding catalytic performance.

The influence of Ni loadings (1-5 wt%) over the Ni/SBA-15 physiochemical properties and CO₂ reforming of CH₄ (CRM) were investigated. The activity of CRM followed the order of 3Ni/SBA-15 > 5Ni/SBA-15 > 2Ni/SBA-15 > 1Ni/SBA-15. Highest

catalytic performance and stability was marked by 3Ni/SBA-15 owing to the well dispersion Ni particles on the SBA-15 surfaces and create a good metal-support interaction (Ni–O–Si) which then offer large amount of basic sites as proved by TEM, FTIR and CO₂-TPD analysis, which then enhance its catalytic performance. The presence of RWGS side reaction over all the Ni/SBA-15 catalysts induced a negative effect towards the hydrogen production, and thus led to less than 1 for H₂/CO ratio. Lowest H₂/CO ratio and catalyst activity stability of 1Ni/SBA-15 were probably due to the larger of Ni particle size (37.96 nm) deposited on the SBA-15 surfaces that favour the RWGS reaction and carbon formation.

Hence, this study affirmed that POFA can be served as silica substitution of Ni/SBA-15. Optimal Ni/SBA-15 was found at Na₂SiO₃-POFA/P123 ratio of 2.9 and Ni loading of 3wt%, with CH₄ conversion = 87.11%, CO₂ conversion = 76.51%, H₂/CO = 0.84.

5.2 Recommendation for future work

Based on the finding and observation of this study, suggestions are recommended to improve for future work. It is recommended to use different silica sources such as rice husk ash, fly ash or sugarcane bagasse ash in catalyst synthesis.

UMP

REFERENCES

- Abdullah, A. Z., Razali, N., & Lee, K. T. (2010). Influence of the Silica-to-Surfactant Ratio and the pH of Synthesis on the Characteristics of Mesoporous SBA-15. *Journal of Physical Science*, 21(2), 13–27.
- Ahmed, R. A., Pang, Y. X., Olea, M., & Hodgson, S. N. B. (2012). Preparation and structural characterisation of SBA-15 supported nickel catalysts via sol-gel nickel oxide coatings for dry reforming of methane, 81, 71–82.
- Alper, E., & Yuksel Orhan, O. (2017). CO₂ utilization: Developments in conversion processes. *Petroleum*, 3(1), 109–126.
- Angeli, S. D., Turchetti, L., Monteleone, G., & Lemonidou, A. A. (2016). Catalyst development for steam reforming of methane and model biogas at low temperature. *Applied Catalysis B: Environmental*, 181, 34–46.
- Arumugam, A., & Ponnusami, V. (2015). Optimization of recovery of silica from sugarcane leaf ash and Ca/SBA-15 solid base for transesterification of Calophyllum inophyllum oil. *Journal of Sol-Gel Science and Technology*, 74(1), 132–142.
- Aziz, M. A. A., Jalil, A. A., Triwahyono, S., Mukti, R. R., Taufiq-Yap, Y. H., & Sazegar, M. R. (2014a). Highly active Ni-promoted mesostructured silica nanoparticles for CO₂ methanation. *Applied Catalysis B: Environmental*, 147(September 2013), 359–368.
- Bamaga, S. O., Hussin, M. W., & Ismail, M. A. (2013). Palm Oil Fuel Ash: Promising supplementary cementing materials. *KSCE Journal of Civil Engineering*, 17(7), 1708–1713.
- Baudouin, D., Rodemerck, U., Krumeich, F., Mallmann, A. De, Szeto, K. C., Ménard, H., Veyre, L., Candy, J. P., Webb, P. B., Thieuleux, C., & Copéret, C. (2013). Particle size effect in the low temperature reforming of methane by carbon dioxide on silica-supported Ni nanoparticles. *Journal of Catalysis*, 297, 27–34.
- Bhagiyalakshmi, M., Yun, L. J., Anuradha, R., & Jang, H. T. (2010a). Synthesis of chloropropylamine grafted mesoporous MCM-41, MCM-48 and SBA-15 from rice husk ash: Their application to CO₂ chemisorption. *Journal of Porous Materials*, 17(4), 475–484.
- Bhagiyalakshmi, M., Yun, L. J., Anuradha, R., & Jang, H. T. (2010b). Utilization of rice husk ash as silica source for the synthesis of mesoporous silicas and their application to CO₂ adsorption through TREN/TEPA grafting. *Journal of Hazardous Materials*, 175(1–3), 928–938.
- Bukhari, S. N., Chin, C. Y., Setiabudi, H. D., & Vo, D. V. N. (2017). Tailoring the properties and catalytic activities of Ni/SBA-15 via different TEOS/P123 mass ratios for CO₂ reforming of CH₄. *Journal of Environmental Chemical Engineering*, 5(4), 3122–3128.
- Chandrasekar, G., Son, W. J., & Ahn, W. S. (2009). Synthesis of mesoporous materials SBA-15 and CMK-3 from fly ash and their application for CO₂ adsorption. *Journal of Porous Materials*, 16(5), 545–551.
- Chandrasekar, G., You, K. S., Ahn, J. W., & Ahn, W. S. (2008). Synthesis of hexagonal

- and cubic mesoporous silica using power plant bottom ash. *Microporous and Mesoporous Materials*, 111(1–3), 455–462.
- Chen, D., Lødeng, R., Anundskås, A., Olsvik, O., & Holmen, A. (2001). Deactivation during carbon dioxide reforming of methane over Ni catalyst: Microkinetic analysis. *Chemical Engineering Science*, 56(4), 1371–1379.
- Chen, L. F., Guo, P. J., Zhu, L. J., Qiao, M. H., Shen, W., Xu, H. L., & Fan, K. N. (2009). Preparation of Cu/SBA-15 catalysts by different methods for the hydrogenolysis of dimethyl maleate to 1,4-butanediol. *Applied Catalysis A: General*, 356(2), 129–136.
- Chiker, F., Nogier, J. P., Launay, F., & Bonardet, J. L. (2003). New Ti-SBA mesoporous solids fonctionalized under gas phase conditions: Characterisation and application to selective oxidation of alkenes. *Applied Catalysis A: General*, 243(2), 309–321.
- Du, G., Lim, S., Pinault, M., Wang, C., Fang, F., Pfefferle, L., & Haller, G. L. (2008). Synthesis, characterization, and catalytic performance of highly dispersed vanadium grafted SBA-15 catalyst. *Journal of Catalysis*, 253(1), 74–90.
- Fazaeli, R., Aliyan, H., Tangestaninejad, S., Mohammadi, E., & Bordbar, M. (2012). Nanocasting, template synthesis, and structural studies on cesium salt of phosphotungstic acid for the synthesis of novel 1, 3, 5-triaryl-pyrazoline derivatives. *Cuihua Xuebao/Chinese Journal of Catalysis*, 33(2), 237–246.
- Fouad, O. A., Mohamed, R. M., Hassan, M. S., & Ibrahim, I. A. (2006). Effect of template type and template/silica mole ratio on the crystallinity of synthesized nanosized ZSM-5. *Catalysis Today*, 116(1), 82–87.
- Fulvio, P. F., Pikus, S., & Jaroniec, M. (2005). Short-time synthesis of SBA-15 using various silica sources. *Journal of Colloid and Interface Science*, 287(2), 717–720.
- Gao, J., Hou, Z., Liu, X., Zeng, Y., Luo, M., & Zheng, X. (2009). Methane autothermal reforming with CO₂ and O₂ to synthesis gas at the boundary between Ni and ZrO₂. *International Journal of Hydrogen Energy*, 34(9), 3734–3742.
- Gupta, N., Gedam, V. V., Moghe, C., & Labhasetwar, P. (2017). Investigation of characteristics and leaching behavior of coal fly ash, coal fly ash bricks and clay bricks. *Environmental Technology and Innovation*, 7, 152–159.
- Haghighi, M., Sun, Z. Q., Wu, J. H., Bromly, J., Wee, H. L., Ng, E., ... Zhang, D. K. (2007). On the reaction mechanism of CO₂ reforming of methane over a bed of coal char. *Proceedings of the Combustion Institute*, 31 II, 1983–1990.
- Han, D., Yeon, S., Wook, S., Kyoung, Y., Jeong, M., Ji, E., & Dok, Y. (2015). Applied Catalysis A : General The catalytic stability of TiO₂ -shell / Ni-core catalysts for CO₂ reforming of CH₄. *Applied Catalysis A, General*, 495, 184–191.
- He, S., He, S., Zhang, L., Li, X., Wang, J., He, D., Lu, J., & Luo, Y. (2015). Hydrogen production by ethanol steam reforming over Ni/SBA-15 mesoporous catalysts: Effect of Au addition. *Catalysis Today*.
- Huang, T., Huang, W., Huang, J., & Ji, P. (2011). Methane reforming reaction with carbon dioxide over SBA-15 supported Ni-Mo bimetallic catalysts. *Fuel Processing Technology*.
- Iskandar, M. J., Baharum, A., Anuar, F. H., & Othaman, R. (2018). Palm oil industry in South East Asia and the effluent treatment technology—A review. *Environmental Technology and Innovation*, 9(May 2017), 169–185.

- Jabbour, K., El Hassan, N., Casale, S., Estephane, J., & El Zakhem, H. (2014). Promotional effect of Ru on the activity and stability of Co/SBA-15 catalysts in dry reforming of methane. *International Journal of Hydrogen Energy*, 39(15), 7780–7787.
- Kathiraser, Y., Oemar, U., Saw, E. T., Li, Z., & Kawi, S. (2015). Kinetic and mechanistic aspects for CO₂ reforming of methane over Ni based catalysts. *Chemical Engineering Journal*, 278, 62–78.
- Kaydouh, M. N., El Hassan, N., Davidson, A., Casale, S., El Zakhem, H., & Massiani, P. (2016). Highly active and stable Ni/SBA-15 catalysts prepared by a “two solvents” method for dry reforming of methane. *Microporous and Mesoporous Materials*, 220, 99–109.
- Kim, J.-H., Suh, D. J., Park, T.-J., & Kim, K.-L. (2000). Effect of metal particle size on coking during CO₂ reforming of CH₄ over Ni–alumina aerogel catalysts. *Applied Catalysis A: General*, 197(2), 191–200.
- Kroehong, W., Sinsiri, T., & Jaturapitakkul, C. (2011). Effect of Palm Oil Fuel Ash Fineness on Packing Effect and Pozzolanic Reaction of Blended Cement Paste. *Procedia Engineering*, 14, 361–369.
- Kruk, M., Jaroniec, M., Joo, S. H., & Ryoo, R. (2003). Characterization of regular and plugged SBA-15 silicas by using adsorption and inverse carbon replication and explanation of the plug formation mechanism. *Journal of Physical Chemistry B*, 107(10), 2205–2213.
- Li, B., & Zhang, S. (2013). Methane reforming with CO₂ using nickel catalysts supported on yttria-doped SBA-15 mesoporous materials via sol-gel process. *International Journal of Hydrogen Energy*, 38(33), 14250–14260.
- Li, D., Zeng, L., Li, X., Wang, X., Ma, H., Assabumrungrat, S., & Gong, J. (2015). Ceria-promoted Ni/SBA-15 catalysts for ethanol steam reforming with enhanced activity and resistance to deactivation. *Applied Catalysis B: Environmental*, 176–177, 532–541.
- Liu, D., Lau, R., Borgna, A., & Yang, Y. (2009). Carbon dioxide reforming of methane to synthesis gas over Ni-MCM-41 catalysts. *Applied Catalysis A: General*, 358(2), 110–118.
- Liu, H., Costa, P. Da, Bel, H., Taief, H., Benzina, M., & G, M. E. (2018). Mg-promotion of Ni natural clay-supported catalysts for dry reforming of methane, 19627–19634.
- Macromoleculas, I. De, Eloisa, P., Universidade, M., Janeiro, R. De, & De, R. (2009). Silica sol obtained from rice husk ash, 3(4).
- Manuscript, A., & Processes, T. (2013). NIH Public Access, 1693, 258–264.
- Miyazawa, K., & Inagaki, S. (2000). Control of the microporosity within the pore walls of ordered mesoporous silica SBA-15. *Chemical Communications*, (21), 2121–2122.
- Moradi, G., Khezeli, F., & Hemmati, H. (2016). Syngas production with dry reforming of methane over Ni/ZSM-5 catalysts. *Journal of Natural Gas Science and Engineering*.
- Norsuraya, S., Fazlena, H., & Norhasyimi, R. (2016). Sugarcane Bagasse as a Renewable Source of Silica to Synthesize Santa Barbara Amorphous-15 (SBA-15). *Procedia*

- Engineering*, 148, 839–846.
- Özdemir, H., Faruk Öksüzömer, M. A., & Ali Gürkaynak, M. (2010). Preparation and characterization of Ni based catalysts for the catalytic partial oxidation of methane: Effect of support basicity on H₂/CO ratio and carbon deposition. *International Journal of Hydrogen Energy*, 35(22), 12147–12160.
- Ozkara, E., Akin, A. N., Misirli, Z., & Aksoylu, A. E. (2005). The Effect of Metal Loading on Structural Characteristics and Low Temperature CO Oxidation Activity of Coprecipitated Co/Al₂O₃. *Turk J Chem*, 29, 219–224.
- Pakhare, D., Shaw, C., Haynes, D., Shekhawat, D., & Spivey, J. (2013). Effect of reaction temperature on activity of Pt- and Ru-substituted lanthanum zirconate pyrochlores (La₂Zr₂O₇) for dry (CO₂) reforming of methane (DRM). *Journal of CO₂ Utilization*, 1, 37–42.
- Pimprom, S., Sriboonkham, K., Dittanet, P., Föttinger, K., Ruppel, G., & Kongkachuichay, P. (2015). Synthesis of copper-nickel/SBA-15 from rice husk ash catalyst for dimethyl carbonate production from methanol and carbon dioxide. *Journal of Industrial and Engineering Chemistry*, 31, 156–166.
- Rahmat, N., Hamzah, F., Sahiron, N., Mazlan, M., & Zahari, M. M. (2016). Sodium silicate as source of silica for synthesis of mesoporous SBA-15. *IOP Conference Series: Materials Science and Engineering*, 133(1).
- Scokart, P. O., & Rouxhet, P. G. (1980). Characterization of the basicity of oxides through the infrared study of pyrrole adsorption. *Journal of the Chemical Society, Faraday Transactions 1: Physical Chemistry in Condensed Phases*, 76, 1476–1489.
- Serrano-Lotina, A., Martin, A. J., Folgado, M. A., & Daza, L. (2012). Dry reforming of methane to syngas over La-promoted hydrotalcite clay-derived catalysts. *International Journal of Hydrogen Energy*, 37(17), 12342–12350.
- Setiabudi, H. D., Chong, C. C., Abed, S. M., Teh, L. P., & Chin, S. Y. (2018). Comparative study of Ni-Ce loading method: Beneficial effect of ultrasonic-assisted impregnation method in CO₂ reforming of CH₄ over Ni-Ce/SBA-15. *Journal of Environmental Chemical Engineering*, 6(1), 745–753.
- Setiabudi, H. D., Jalil, A. A., Triwahyono, S., Kamarudin, N. H. N., & Mukti, R. R. (2012). IR study of iridium bonded to perturbed silanol groups of Pt-HZSM₅ for n-pentane isomerization. *Applied Catalysis A: General*, 417–418, 190–199.
- Setiabudi, H. D., Lim, K. H., Ainirazali, N., & Chin, S. Y. (2017). CO₂ reforming of CH₄ over Ni / SBA-15 : Influence of Ni loading on the metal- support interaction and catalytic activity. *Journal of Materials and Environmental Sciences*, 8(2), 573–581.
- Setiabudi, H. D., Razak, N. S. A., Suhaimi, F. R. M., & Pauzi, F. N. (2016). CO₂ reforming of CH₄ over Ni/SBA-15: Influence of Ni-loading methods. *Malaysian Journal of Catalysis*, 1, 1–6.
- Sidik, S. M., Triwahyono, S., Jalil, A. A., Aziz, M. A. A., & Fatah, N. A. (2016). Tailoring the properties of electrolyzed Ni/mesostructured silica nanoparticles (MSN) via different Ni-loading methods for CO₂ reforming of CH₄. *Journal of CO₂ Utilization*, 13, 71–80.
- Sidik, S. M., Triwahyono, S., Jalil, A. A., Aziz, M. A. A., Fatah, N. A. A., & Teh, L. P. (2016). Tailoring the properties of electrolyzed Ni/mesostructured silica

- nanoparticles (MSN) via different Ni-loading methods for CO₂ reforming of CH₄. *Journal of CO₂ Utilization*, 13, 71–80.
- Silva, R. J. farias da, Dutra, A. J. B., & Afonso, J. C. (2012). Hydrometallurgy Alkali fusion followed by a two-step leaching of a Brazilian zircon concentrate. *Hydrometallurgy*, 117–118, 93–100.
- Sing, K. S. W., Everett, D. H., Haul, R. A. W., Moscou, L., Pierotti, R. S., Rouquerol, J., & Siemieniewska, T. (1985). International union of pure commission on colloid and surface chemistry including catalysis-Reporting physisorption data for gas/solid systems with special reference to the determination of surface area and porosity. *Pure & Appl. Chem.*, 57(4), 603–619.
- Taherian, Z., Yousefpour, M., Tajally, M., & Khoshandam, B. (2017). Catalytic performance of Samaria-promoted Ni and Co/SBA-15 catalysts for dry reforming of methane. *International Journal of Hydrogen Energy*, 42(39), 24811–24822.
- Taufiq-Yap, Y. H., Sudarno, Rashid, U., & Zainal, Z. (2013). CeO₂-SiO₂ supported nickel catalysts for dry reforming of methane toward syngas production. *Applied Catalysis A: General*, 468, 359–369.
- Tomishige, K., Chen, Y. G., & Fujimoto, K. (1999). Studies on carbon deposition in CO₂ reforming of CH₄ over nickel-magnesia solid solution catalysts. *Journal of Catalysis*, 181(1), 91–103.
- Usman, M., Wan Daud, W. M. A., & Abbas, H. F. (2015). Dry reforming of methane: Influence of process parameters - A review. *Renewable and Sustainable Energy Reviews*, 45, 710–744.
- Vafaeian, Y., Haghghi, M., & Aghamohammadi, S. (2013). Ultrasound assisted dispersion of different amount of Ni over ZSM-5 used as nanostructured catalyst for hydrogen production via CO₂ reforming of methane. *Energy Conversion and Management*, 76, 1093–1103.
- Wang, J., Fang, L., Cheng, F., Duan, X., & Chen, R. (2013). Hydrothermal synthesis of SBA-15 using sodium silicate derived from coal gangue. *Journal of Nanomaterials*, 2013, 2–7.
- Wang, N., Yu, X., Shen, K., Chu, W., & Qian, W. (2013). Synthesis, characterization and catalytic performance of MgO-coated Ni/SBA-15 catalysts for methane dry reforming to syngas and hydrogen. *International Journal of Hydrogen Energy*, 38(23), 9718–9731.
- Wang, S., Wang, Y., & Hu, C. (2018). The effect of NH₃·H₂O addition in Ni/SBA-15 catalyst preparation on its performance for carbon dioxide reforming of methane to produce H₂. *International Journal of Hydrogen Energy*, 1–10.
- Wang, Y., Chen, G., Zhang, F., & Li, L. (2014). Effect of pH on the structural characteristics of in situ synthesized Ni-incorporated SBA-15 magnetic composites. *Research on Chemical Intermediates*, 40(1), 385–397.
- Ye, W., Lin, Z., Dong, B., Kang, J., Zheng, X., & Wang, X. (2011). Preparation and Catalytic Properties of Ti-SBA-15 Mesoporous Materials. *Material Science and Application*, 2, 661–668.
- Yılmaz, M. S., Pişkin, S., & Materials, A. (2013). Extraction of Silicon from Tailings Slurry of Gold Mine Treatment Plant by Alkali Fusion Technique, 1(2), 2–4.

- Zhang, J., Wang, H., & Dalai, A. K. (2008). Effects of metal content on activity and stability of Ni-Co bimetallic catalysts for CO₂ reforming of CH₄. *Applied Catalysis A: General*, 339(2), 121–129.
- Zhang, J., Wang, H., & Dalai, A. K. (2009). Kinetic Studies of Carbon Dioxide Reforming of Methane over Ni-Co/Al-Mg-O Bimetallic Catalyst. *Industrial & Engineering Chemistry Research*, 48(2), 677–684.
- Zhang, L., Li, L., Li, J., Zhang, Y., & Hu, J. (2014). Carbon dioxide reforming of methane over nickel catalyst supported on MgO(111) nanosheets. *Topics in Catalysis*, 57(6–9), 619–626.
- Zhang, M., Ji, S., Hu, L., Yin, F., Li, C., & Liu, H. (2006). Structural characterization of highly stable Ni/SBA-15 catalyst and its catalytic performance for methane reforming with CO₂. *Chinese Journal of Catalysis*, 27(9).
- Zhang, S., Wang, J., Liu, H., & Wang, X. (2008). One-pot synthesis of Ni-nanoparticle-embedded mesoporous titania/silica catalyst and its application for CO₂-reforming of methane. *Catalysis Communications*, 9(6), 995–1000.
- Zhao, D., Feng, J., Huo, Q., Melosh, N., Glenn, H. F., Chmelka, B. F. & Stucky, G. D. (2016). Triblock Copolymer Syntheses of Mesoporous Silica with Periodic 50 to 300 Angstrom Pores. *Science*, 279(5350), 548–552.
- Zhu, K., Hua, W., Deng, W., & Richards, R. M. (2012). Preparation of MgO nanosheets with polar (111) surfaces by ligand exchange and esterification - Synthesis, structure, and application as catalyst support. *European Journal of Inorganic Chemistry*, (17), 2869–2876.
- Zhu, M., Lerum, M. Z., & Chen, W. (2012). How to Prepare Reproducible, Homogeneous and Hydrolytically. *Langmuir*, 28(1), 416–423.

The logo for UMP (University of Montpellier) is a large, stylized letter 'M' composed of several overlapping triangles in shades of blue, teal, and yellow. The letters 'UMP' are printed in white, bold, sans-serif font across the center of the 'M' shape.

UMP

RESEARCH OUTPUT

List of Publications

1. S.N. Bukhari, C.Y. Chin, H.D. Setiabudi, D.V.N. Vo, Tailoring the properties and catalytic activities of Ni/SBA-15 via different TEOS/P123 mass ratios for CO₂ reforming of CH₄, *Journal of Environmental Chemical Engineering*, 5(4) (2017) 3122-3128. (ISSN: 2213-3437, Indexed Journal, SJR: 0.924)
2. H.D. Setiabudi, C.C. Chong, S.M. Abed, L.P. Teh, S.Y. Chin, Comparative study of Ni-Ce loading method: Beneficial effect of ultrasonic-assisted impregnation method in CO₂ reforming of CH₄ over Ni-Ce/SBA-15, *Journal of Environmental Chemical Engineering* 6(1) (2018) 745-753. (ISSN: 2213-3437, Indexed Journal, SJR: 0.924)
3. S.N. Bukhari, C.C. Chong, L.P. Teh, D.V.N. Vo, N. Ainirazali, S. Triwahyono, A.A. Jalil, H.D. Setiabudi, Promising hydrothermal technique for efficient CO₂ methanation over Ni/SBA-15, *International Journal of Hydrogen Energy*. (ISSN: 0360-3199, ISI Journal, IF = 4.229, Available Online, <https://doi.org/10.1016/j.ijhydene.2018.07.018>)
4. C.C. Chong, N. Abdullah, S.N. Bukhari, N. Ainirazali, L.P. Teh, H.D. Setiabudi, Hydrogen production via CO₂ reforming of CH₄ over low-cost Ni/SBA-15 from silica-rich palm oil fuel ash (POFA) waste, *International Journal of Hydrogen Energy*. (ISSN: 0360-3199, ISI Journal, IF = 4.229, Available Online, <https://doi.org/10.1016/j.ijhydene.2018.06.169>)
5. H.D. Setiabudi, N.S.A. Razak, F.R.M. Suhaimi, F.N. Pauzi, CO₂ reforming of CH₄ over Ni/SBA-15: Influence of Ni-loading methods, *Malaysian Journal of Catalysis* 1 (2016) 1-6. (Non-Indexed Journal)

List of Conferences

1. Bukhari, S. N., Owgi, A. H. K., Ainirazali, N., Vo, D. N., & Setiabudi, H.D. (2017). Enhanced catalytic performance of Ni/SBA-15 towards CO₂ methanation via P123-assisted method. *The 3rd International Conference on Green Chemical Engineering and Technology (3rd GCET)*: 07-08 November 2017, Melaka,

- Malaysia. (Accepted in Material Today: Proceedings, ISSN: 2214-7853, Indexed Journal, SJR: 0.314).
2. C.C. Chong, A.H.K. Owgi, N. Ainirazali, S.Y. Chin, H.D. Setiabudi, CO₂ Reforming of CH₄ over Ni/SBA-15 Prepared by Surfactant-Assisted Impregnation Method: Comparative Study of Surfactant Types. *The 3rd International Conference on Green Chemical Engineering and Technology (3rd GCET)*: 07-08 November 2017, Melaka, Malaysia. (Accepted in Material Today: Proceedings, ISSN: 2214-7853, Indexed Journal, SJR: 0.314).
 3. N. Abdullah, C.C. Chong, H.A. Razak, N.Ainirazali, S.Y. Chin, H.D. Setiabudi, Synthesis of Ni/SBA-15 for CO₂ Reforming of CH₄: Utilization of Palm Oil Fuel Ash as Silica Source. *The 3rd International Conference on Green Chemical Engineering and Technology (3rd GCET)*: 07-08 November 2017, Melaka, Malaysia. (Accepted in Material Today: Proceedings, ISSN: 2214-7853, Indexed Journal, SJR: 0.314).

Exhibitions

1. Chin Chia Yun, Herma Dina Setiabudi, Design and development of Ni/SBA-15 for CO₂ reforming of CH₄, 2016 Creation, Innovation, Technology & Research Exposition (CITREX 2016), 7-8 March 2016, Universiti Malaysia Pahang, Pahang. (Bronze)
2. Lim Kiang Hoo, Herma Dina Setiabudi, Nurul Aini Mohamed Razali, Development of Ni/SBA-15 catalyst and its potential in enhancing syngas production, 2016 Creation, Innovation, Technology & Research Exposition (CITREX 2016), 7-8 March 2016, Universiti Malaysia Pahang, Pahang. (Bronze)
3. C.C. Chong, N. Abdullah, S.N.M. Bukhari, N.A. Razali, H.D. Setiabudi, Ni/SBA-15(POFA) from palm oil fuel ash for CO₂ reforming of CH₄, 2017 Creation, Innovation, Technology & Research Exposition (CITREX 2017), 15-16 March 2017, Universiti Malaysia Pahang, Pahang. (Silver)

List of Students

Master Research

1. Nornasuha Abdullah (MKC16030), Utilization of Palm Oil Fuel Ash as Silica Source of Ni/SBA-15 For Carbon Dioxide Reforming of Methane, Master Research, 2018.

Undergraduate Research Project

1. Chong Chi Cheng (KE13040), Synthesis and Characterization of Ni/SBA-15 From POFA for CO₂ Reforming of CH₄: Effect of POFA Sodium Silicate/P123 Mass Ratio, Undergraduate Research Project, 2016.
2. Khaw Chee Sean (KA13091), Synthesis and Characterization of Ni/SBA-15 From POFA for CO₂ Reforming of CH₄: Effect of POFA Sodium Silicate/Commercial Sodium Silicate, Undergraduate Research Project, 2016.



UMP